

Cellular mechanism of absence epilepsy  
in calcium channel mutant mice

Sachie Sasaki

Department of Physiological Sciences

School of Life Science

The Graduate University for Advanced Studies

# CONTENTS

Abstract	1
Introduction	3
Experimental Procedures	6
Results	14
Discussion	30
References	41
Acknowledgments	48
Figures and Figure Legends	

## Abstract

Homozygous *tottering* (*tg*) mice have a mutation in the voltage-dependent Cav2.1 (P/Q-type) Ca<sup>2+</sup> channel  $\alpha_12.1$  subunit gene. *tg* mice show not only cerebellar ataxia but also absence epilepsy, which begins at about 3 weeks of age and persists throughout life. Similarities in EEG and pharmacological sensitivity suggest that *tg* mice can serve as a model of human absence epilepsy. To identify the mechanism of epileptogenesis, I studied the effect of the mutation on the thalamocortical network using whole-cell patch clamp recordings in brain slice preparations. IPSC amplitudes recorded from layer IV pyramidal cells of the cerebral cortex in response to thalamic stimulation became disproportionately reduced, compared with EPSC amplitudes, in the later developmental stage (P21-30). Similar results were obtained by local stimulation in layer IV pyramidal neurons. However IPSC reduction was not seen in layer V pyramidal neurons or in layer IV pyramidal neurons of younger *tg* mice before the onset of epilepsy (P14-16). Furthermore, recordings of multiple field potentials revealed that cortical excitation (evoked by layer IV stimulation) spread in the horizontal direction more strongly in epileptic *tg* than in control or non-epileptic *tg* mice. These results demonstrated a close relationship between impaired IPSCs in layer IV and absence epilepsy, and suggested that the defect of feed-forward inhibition in the cortical input layer is critically involved

in the generation of absence epilepsy in *tg* mice.

## **Introduction**

Absence seizures are one type of generalized epilepsy. They are easily characterized by bilaterally synchronous spike-and-wave discharges (SWDs) in the electroencephalogram (EEG) over wide cortical areas. In humans, depth electrode recordings from the thalamus revealed that the SWDs are generated in the thalamocortical network (Williams, 1953). These results led to the hypothesis that an aberration of the interplay between the cerebral cortex and the thalamus causes the SWDs. The relative contribution of the thalamus and the cortex to the pathophysiological conditions has been a matter of severe debate for decades.

The generalized nature of the SWDs over wide cortical areas implies the thalamic contribution to the absence seizure. The massive thalamic synchronization results from recurrent oscillatory activity in the networks between thalamocortical relay cells and cells of the reticular thalamic nucleus (Buzsaki, 1991; McCormick and Bal, 1997; Avanzini et al., 2000). On the other hand, some researchers have stressed the important role of intracortical processes in the SWDs (Meeren et al., 2002). In this study, I attempted to reveal the mechanism of spontaneously occurring generalized SWDs by using thalamocortical slice preparations in an established genetic model of absence seizure, homozygous *tg* mice (Noebels and Sidman, 1979).

In homozygous *tg* mice, positional cloning techniques were used to identify the gene causing the neurological disorders consisting of ataxia and absence seizure: the gene encoding the  $\alpha_12.1$  subunit of the voltage-gated calcium channels (Fletcher et al., 1996; Mori et al., 2000). These findings permitted investigations of the molecular mechanisms through which this gene mutation causes neurological disorders. The  $\alpha_12.1$  subunit forms the channel pore of the  $Ca_v2.1$  (P/Q type) calcium channels (Mori et al., 1991; Starr et al., 1991; Sather et al., 1993; Zhang et al., 1993; Stea et al., 1994; Randall and Tsien, 1995), which plays essential roles in a variety of functions including neurotransmitter release at presynaptic sites. Extensive studies on the mutated  $Ca_v2.1$  channel in the native cerebellar Purkinje cells as well as in the recombinant express systems revealed that the *tg* mutation reduced the calcium influx through the channel (Wakamori et al., 1998). The absence seizure in *tg* mice resembles human absence epilepsy, but the mechanism responsible for the seizure has remained unknown.

Based on a number of *in vitro* and *in vivo* studies, it has been thought that an imbalance between excitation and inhibition within the thalamocortical loop might be critical for genesis of absence seizure (Gllor et al, 1990; for review, see Manning, 2003). To determine whether the *tg* mutation of the  $Ca_v2.1$  calcium channel directly alters the excitability of thalamocortical networks, and to localize where in this circuit the

functional defect may be expressed, we examined cortical neurons in thalamocortical brain slice preparations with the use of whole cell voltage-clamp recordings. Here I describe that inhibitory synaptic transmission to layer IV pyramidal neurons is disproportionately impaired in *tg* mice. The present results suggest that derangement of the cortical network at thalamocortical inputs is critical to generation of absence seizure.

## **Experimental Procedures**

*Animals.* The C57BL/6-tg strain of *tottering* (*tg*) mice was introduced from the Jackson Laboratory (Bar Harbor, ME, USA). C57BL/6 mice were used as wild-type control (wt). Mice at postnatal days (P) 14-30 were used for the experiments. Mice were provided with a commercial diet (CE-2, Nihon Clea, Tokyo, Japan) and water *ad libitum* under conventional conditions with controlled temperature, humidity, and lighting ( $22 \pm 2^\circ\text{C}$ ,  $55 \pm 5\%$ , and 12-h light/dark cycle with lights on at 6 A.M.). The strain was maintained and propagated by mating between heterozygous mice. All animal studies described in this work were reviewed and approved by the ethical committee in our institute and were performed according to the institutional guidelines concerning the care and handling of experimental animals.

*Genotyping of tg mice.* Genomic DNA was extracted from the tail as follows: a mouse tail tip 2 mm in length was cut and put into a 0.5-ml tube with safety lock. The sample was heated at  $96^\circ\text{C}$  for 10 min, and then treated with proteinase K (Invitrogen, Carlsbad, CA, USA) at  $55^\circ\text{C}$  for 90 min. The genomic region encoding a part of the calcium channel  $\alpha_{1.2.1}$  subunit gene was amplified using the cDNA polymerase mix (Clontech, Palo Alto, CA, USA) and two sets of PCR primers, which were 5'-TTAATTTTGATGAAGGGACTCC-3' (sense for wt mice),

5'-TTAATTTTGATGAAGGGACTCT-3'(sense for *tg* mice) and 5'-CCAGCAACAATGAAAACAAGCATTCCAAAACAGC-3' (anti-sense for both wt and *tg*). The DNA-extracted solution (2  $\mu$ l) was used as a template for PCR. The PCR parameters consisted of 28 cycles of 94°C for 30 s, 55°C for 30 s, and 72°C for 30 s, and final extension of 72°C for 7 min. The resulting PCR products were subjected to electrophoresis on a 2.0% agarose gel.

*Slice preparation.* The procedure for preparing thalamocortical slices was modified from the method described by Agmon and Connors (1991). Mice were killed by decapitation under deep halothane general anesthesia. Brains were removed from wt and *tg* mice and put into ice-cold cutting solution containing (in mM): 120 choline-Cl, 3 KCl, 1.25 NaH<sub>2</sub>PO<sub>4</sub>, 28 NaHCO<sub>3</sub>, 8 MgCl<sub>2</sub>, and 22 glucose, saturated with carbogene (95% O<sub>2</sub> and 5% CO<sub>2</sub>). The tissue was cut into 350-450  $\mu$ m-thick slices with a vibratome (VT1000S; Leica, Nussloch, Germany). The slices were then incubated at 32°C for 30 min and room temperature for at least 30 min in artificial CSF (ACSF) containing (in mM): 125 NaCl, 25 NaHCO<sub>3</sub>, 25 glucose, 2.5 KCl, 1.25 NaH<sub>2</sub>PO<sub>4</sub>, 2 CaCl<sub>2</sub>, and 1 MgCl<sub>2</sub>, bubbled with carbogene.

*Electrophysiological recordings.* A whole-cell voltage-clamp recording was made from layer IV and V pyramidal neurons of the mouse barrel cortex, which were visually

identified using an upright microscope equipped with a x 60 water immersion objective (BX51WI, Olympus Optical, Tokyo, Japan) and an infrared differential interference contrast video system (C2400-79H, Hamamatsu Photonics, Hamamatsu, Japan). Patch pipettes were made from borosilicate capillaries (2.0 mm outer diameter and 1.0 mm inner diameter; Hilgenberg, Malsfeld, Germany). Excitatory postsynaptic currents (EPSCs) and inhibitory postsynaptic currents (IPSCs) were recorded with an EPC9 patch-clamp amplifier (HEKA, Lambrecht, Germany). The access resistance for recording was  $< 15 \text{ M}\Omega$  and compensated by 50-70%. Cells were rejected if access resistance increased above  $15 \text{ M}\Omega$ . Stimulation and data acquisition were performed using the PULSE program (version 8.54, HEKA). The current signals were filtered at 3 kHz and digitized at 20 kHz. The experiments were performed at a bath temperature of  $32^\circ\text{C}$ .

*Thalamocortical response.* Thalamocortical EPSCs and IPSCs were evoked by electrical stimulation (10 mA, 200  $\mu\text{s}$ ), using a stimulus isolator (ISO-FLEX, A.M.P.I., Jerusalem, Israel) and stainless steel bipolar semi-microelectrodes (A-M Systems, Carlsborg, WA, USA) placed in the ventrobasal (VB) thalamic nucleus or the internal capsule (Fig. 1A). Patch pipettes (3-6  $\text{M}\Omega$ ) were filled with an internal solution containing (mM): 122 Cs- $\text{CH}_3\text{SO}_3$ , 5 KCl, 0.1 EGTA, 10 HEPES, 3 Mg-ATP and 0.4

Na-GTP (adjusted to pH 7.4 with CsOH). QX-314 (final 5 mM) was added to prevent Na<sup>+</sup> spike generation. APV (100 μM) was added to the external solution, to block NMDA receptor-mediated currents, which otherwise often masked IPSCs. EPSCs were recorded at a holding potential of -60 mV, whereas IPSCs were recorded at 0 mV, which was close to reversal potentials of glutamate receptor mediated currents.

*Local response.* IPSCs and EPSCs were evoked by local electrical stimulation (0.1-10 mA, 200 μs), using a bipolar tungsten microelectrode with these tips of the distance of 100 μm. The stimulation electrode was usually placed at about 100 μm (vertically deeper) from the soma of a pyramidal cell. The resistance of patch pipettes was 3-6 MΩ when filled with intracellular solutions. The internal solution for measuring IPSCs contained (mM): 140 CsCl, 9 NaCl, 1 EGTA, 10 HEPES and 2 Mg-ATP (adjusted to pH 7.3 with CsOH). The internal solution for measuring EPSCs contained (mM): 115 K-gluconate, 20 KCl, 1 EGTA, 10 HEPES, 4 Mg-ATP, 0.3 Na-GTP and 10 phosphocreatine (adjusted to pH 7.4 with KOH). QX-314 (final 5 mM) was added to prevent Na<sup>+</sup> spike generation.

*Miniature IPSCs.* For recording miniature IPSCs (mIPSCs) in layer IV pyramidal neurons, slices from P21-27 wt and *tg* mice were bathed in ACSF containing 1 μM TTX, 10 μM CNQX, and 100 μM APV. The holding potential was -60 mV. Currents were

filtered at 3 kHz and digitized at 5 kHz. Series resistance was measured periodically.

Off-line data analysis of peak amplitudes was performed with an IgorPro program (Wavemetrics, Lake Oswego, OR, USA). Peak amplitudes were measured at the absolute maximum of the currents, taking into account the noise of the baseline and noise around the peak.

*Morphological identification.* For morphological characterization of individual recorded neurons, 0.5% biocytin (Sigma, St. Louis, MO, USA) was included in the internal solutions. After fixing overnight with 4% paraformaldehyde and rinsing with 0.05M sodium phosphate buffered saline (PBS), the slices were incubated for 30 min with 400  $\mu$ l of 30% H<sub>2</sub>O<sub>2</sub> in 20 ml methanol. And after rinsing with PBS and permeabilizing with 0.3% Triton X-100, the slices were incubated for 3 hr with ABC solution (Vector Laboratories, Burlingame, CA, USA). After two rinses in PBS and two rinses in 0.05M Tris-HCl-buffered saline (TBS), the slices were preincubated with 0.7 mg/ml of 3'3'-diaminobenzidine (DAB; Sigma) for 30 min, and then the reaction was initiated by adding 0.3% H<sub>2</sub>O<sub>2</sub>. The reaction was stopped by TBS for 10 min, and two rinses with PBS. To identify the barrel cortex, the slices were incubated for 20 sec with methylgreen after mounting onto a gelatin-coated slideglass.

*Histological procedure.* For immunohistochemistry, wt and tg mice aged P21-23 were

anesthetized with 75 mg/kg pentobarbital, perfused intracardially with 4% paraformaldehyde and 0.2% picric acid in 0.1 M sodium phosphate buffer (PB) for 12 min. Brains were removed and fixed for an additional overnight at 4°C, and subsequently incubated in PB containing 10%, 20% and 30% sucrose for overnight each. The tissue was sliced at 40 µm along the coronal section by a microtome (SM2000R; Leica). Tissue slices were washed in 0.05 M TBS before incubation in 1% H<sub>2</sub>O<sub>2</sub> for 1hr. Slices were washed three times in TBS and incubated with a rabbit polyclonal antibody against GAD (Chemicon, Temecula, CA, USA; 1:5000) in TBS containing 10% normal goat serum and 2% bovine serum albumin for 2 overnight at 4°C. The tissue was washed three times in TBS and incubated 3 hr at room temperature in biotinylated anti-rabbit IgG (Vector Laboratories) using a 1:200 final dilution including normal goat serum and TBS. After rinses, the tissue was incubated with avidine-biotin-peroxidase complex (ABC Elite kit; Vector Laboratories) in TBS for 30 min. After washing in TBS, the tissues were reacted with DAB (0.05%) and H<sub>2</sub>O<sub>2</sub> (0.002%) in TBS. They were then post-fixed for 30 min in 1% OsO<sub>4</sub> in PB, dehydrated in graded ethanol, and flat-embedded on glass slides in Epon. Immunostaining clearly stained the somata of GABAergic neurons, sparing their nuclei. Density of the stained cells were measured in at least 1-mm-wide vertical strips in layer IV barrel cortex (typically 300 µm height x

1,000  $\mu\text{m}$  width). To ascertain the barrel cortex, alternate sections were stained for Nissle and GAD.

*MED64 system.* Procedures for the preparation of the recently introduced Multi-Electrode Dish (MED probes; Panasonic, Osaka, Japan) were described by Oka et al. (1999). The device has an array of 64 planar microelectrodes, each having a size of 50 x 50  $\mu\text{m}$ , arranged in an 8 x 8 pattern (Panasonic; MED-P2105). For sufficient adhesion of the slice to the probe, the surface of the MED probe was treated with 0.1% polyethylenimine (Sigma) in 15 mM borate buffer, pH 8.4, for 8 hr at room temperature. The probe surface was rinsed three times with sterile distilled water. The probe was then filled with DMEM medium, containing 10% fetal bovine serum (Life Technologies, Gaithersburg, MD, USA; 16141-079) and 10% horse serum (Life Technologies; 16050-122), for at least 1 hr at 37°C. The probe surface was rinsed three times with sterile distilled water. During electrophysiological recording, the slices on the MED probe were bathed in ACSF with carbogene. The experiments were performed at a bath temperature of 32°C.

Evoked local field potentials at all 64 sites, using MED64 system (Alpha MED Sciences, Tokyo, Japan), were recorded simultaneously at a 20 kHz sampling rate (Fig. 9B). I made stimulations at individual barrels by placing the tip of the stimulus-pipette

in the center of the barrel. The microelectrode used for extracellular stimulation was an ACSF-filled double-barrel micropipette (TGC200-10  $\theta$ -glass; Harvard Apparatus, Kent, UK) with tip diameters of 10-14  $\mu\text{m}$ . Bipolar constant-current pulses (0.1-0.5 mA; 0.1 msec) were produced by the isolated stimulator, which was controlled via the data acquisition software.

*Data analysis and statistics.* All values are given as means  $\pm$  SEMs. Statistical comparison between wt and *tg* mice was performed by t test (\*  $p < 0.05$ , \*\*  $p < 0.01$ ).

Data analysis and fitting procedures were performed using IgorPro. The values of IPSC and EPSC peak amplitudes were obtained from averages of 5-10 consecutive traces.

*Chemicals.* 6-cyano-7-nitroquinoxaline-2,3-dion (CNQX), DL-2-amino-5-phosphonopentanoic acid (APV) and picrotoxin were obtained from Sigma. Tetrodotoxin (TTX) was obtained from Sankyo (Tokyo, Japan). (-)- Bicuculline methochloride (bicuculline) was obtained from Tocris (Avonmouth, UK). All other chemicals were from Nacalai Tesque (Kyoto, Japan) or Wako Pure Chemical Industries (Osaka, Japan), unless specified otherwise.

## **Results**

### **Thalamocortical response in adult wt and *tg* mice**

In the somatosensory cortex, layer IV is the main input gateway for afferent fibers originating in the respective thalamic relay nuclei (Hubel and Wiesel, 1962; McGuire et al., 1984; Chiaia et al., 1991a,b; for review, see Sherman and Guillery, 1996). In layer IV, two morphologically different excitatory neurons are present. They are spiny stellate cells and pyramidal cells (Simons and Wooley, 1984). The two cell types play different roles in the barrel cortex. Pyramidal neurons show stronger responses to multi-whisker stimulation than spiny stellate cells in an *in vivo* study (Brecht and Sakmann, 2002). Spiny stellate cells act predominantly as local signal processors within a single barrel, whereas pyramidal cells globally integrate horizontal and top-down information within a functional column and between neighboring barrels (Schubert et al., 2003). Because it was technically easier to identify pyramidal cells than spiny stellate cells in the slice preparation under the DIC-video microscopy, I focused on the layer IV pyramidal cells in this study, so that I could study a relatively homogenous neuronal population. Furthermore, in this study, I used thalamocortical brain preparations, which were unique in including both the ventrobasal nucleus (VB) of the thalamus and the somatosensory (barrel) cortex with the functional connectivity between them.

Voltage-clamp recordings were made from layer IV pyramidal cells in of the somatosensory cortex (barrel cortex) in the whole-cell patch clamp configuration (Fig. 1A). Most of the recorded neurons were examined morphologically by including 0.5% biocytin in the pipette and staining after electrophysiological recordings. They were identified as pyramidal cells (Fig. 1B). Excitatory post-synaptic currents (EPSCs) and inhibitory post-synaptic currents (IPSCs) were evoked by thalamic stimulation, and EPSC and IPSC were compared between wt and epileptic *tg* mice (P21-30) (Fig. 1C and D).

The current traces recorded from pyramidal cells indicated that they received an excitatory thalamocortical input of non-NMDA receptor-mediated currents, because the recordings were made in presence of an NMDA receptor antagonist DL-2-amino-5-phosphonopentanoic acid (APV, 100  $\mu$ M). APV was used because large NMDA receptor-mediated currents often masked IPSC when they were recorded at a holding potential of 0 mV (see below). When the holding potential was -60 mV, prominent EPSCs were recorded in layer IV pyramidal cells (Fig 1C; *upper trace*). When the holding potential was 0 mV, EPSCs became very small, and there appeared outward currents (Fig 1C; *lower trace*). The outward currents were GABA<sub>A</sub> receptor-mediated IPSCs, because they were completely blocked by GABA<sub>A</sub> receptor antagonist (-)-

bicuculline methochloride (bicuculline) (10  $\mu$ M) or picrotoxin (50  $\mu$ M) (data not shown). Both EPSCs and IPSCs were completely abolished at 0 mV by non-NMDA receptor antagonist 6-cyano-7-nitroquinoxaline-2,3-dione (CNQX, 10  $\mu$ M) (data not shown). This observation suggested that the IPSCs were mediated by a disynaptic response, i.e., by inhibitory interneurons excited by excitatory thalamocortical inputs. EPSCs were mainly monosynaptic responses because the synaptic delay between the stimulation and the onset of EPSCs was short ( $2.1 \pm 0.13$  ms;  $n = 12$ ). The onset of IPSCs followed the onset of EPSCs in every preparation. I only accepted recordings from pyramidal cells where the delay between the onset of monosynaptic EPSCs and the onset of disynaptic IPSCs was more than 1 ms. The mean delay between the onsets of EPSCs and IPSCs was  $1.3 \pm 0.08$  ms ( $n = 12$ ). Fig. 1E shows the relationship between the EPSC and IPSC amplitudes obtained from individual cells, in which the amplitude of EPSC ranged from 100 pA to 500 pA in both wt and *tg* mice. The IPSC amplitude in wt became larger with increasing EPSC amplitude, although the amplitudes were quite variable. In contrast, the IPSC amplitude was very small with a large EPSC in *tg* mice. The slope of linear least-square fitting of the EPSC-IPSC relationship was significantly different between wt and *tg* mice (2.52 for wt and 0.36 for *tg*). The ratio of the peak amplitude of IPSC at 0 mV to that of EPSC at -60 mV was

used as an index for the relative strength of IPSC to EPSC (Fig. 1F). The IPSC/EPSC ratio was greatly reduced in *tg* ( $0.45 \pm 0.06$ ;  $n = 11$ ) compared with wt mice ( $2.29 \pm 0.61$ ;  $n = 12$ ;  $**p < 0.01$ ). These results demonstrated that thalamocortical inhibitory responses were disproportionately decreased in layer IV pyramidal cells of *tg* mice, resulting in an excitation-dominant condition.

### **Locally evoked IPSCs and EPSCs**

Thalamocortical responses recorded in layer IV pyramidal cells were complex, consisting of at least two components of monosynaptic EPSCs and disynaptic IPSCs.

The lags of the synaptic onsets between two types of responses were close.

Pharmacological blockade of EPSCs also abolished IPSCs. These facts made it difficult to evaluate synaptic currents quantitatively, especially IPSCs. To circumvent this problem, I measured IPSCs and EPSCs evoked by local stimulation within the somatosensory cortex. The stimulating electrode was placed at about 100  $\mu\text{m}$  from the soma of recorded pyramidal cells.

Layer IV pyramidal cells were voltage-clamped at  $-60$  mV, and amplitudes of evoked responses to local stimulation were recorded in the presence of CNQX (10  $\mu\text{M}$ ) and APV (100  $\mu\text{M}$ ) for IPSCs, and in the presence of bicuculline (10  $\mu\text{M}$ ) for EPSCs.

For measuring IPSCs, a pipette solution with a high chloride concentration was used so that IPSCs were observed as inward currents. IPSCs were blocked by bicuculline in both wt and *tg* mice (data not shown). The IPSCs or EPSCs were compared between wt and *tg* mice at P21-30.

Layer IV pyramidal cells receive inputs from a large number of interneurons. This fact made it difficult to compare IPSCs amplitudes in different slice preparations. To minimize this problem, I locally stimulated at a constant location, and changed intensity of stimulation to obtain the current amplitude-stimulation intensity relationship (Fig. 2A).

Local stimulation easily evoked large IPSCs in wt mice at P21-30 ( $1,213 \pm 313$  pA;  $n = 11$ , 1.0 mA stimulation). In contrast, the IPSC amplitudes evoked by local stimulation was drastically reduced by 92% in *tg* mice at P21-30 ( $96.4 \pm 21.7$  pA;  $n = 12$ , 1.0 mA stimulation;  $**p < 0.01$ ; Fig. 2C). Moreover, increasing the stimulation intensity was less effective to elicit longer IPSCs in layer IV pyramidal cells of *tg* mice (stimulation intensity 0.1-10 mA) (Fig. 2A). On the other hand, the EPSC amplitudes evoked by local stimulation increased gradually with increment of stimulation intensity in both wt and *tg* mice (Fig. 2B). The averaged EPSC amplitudes were not significantly different between wt ( $790 \pm 222$  pA;  $n = 11$ , 10 mA stimulation) and *tg* mice ( $559 \pm 158$

pA;  $n = 11$ , 10 mA stimulation;  $p > 0.05$ , Fig. 2D). These results suggested that the inhibitory synaptic transmission to layer IV pyramidal neurons was severely impaired in *tg* mice, causing the disproportionately excitation-dominant thalamocortical responses in the cortical input layer.

### **Miniature IPSCs in layer IV pyramidal neurons**

The responses evoked by local stimulation demonstrated that inhibitory synaptic transmission onto layer IV pyramidal neurons was drastically impaired in epileptic *tg* mice. The site of the impairment could be presynaptic or postsynaptic. One possibility was that neurotransmitter release from presynaptic terminals was not functional in *tg* mice, because of the mutation of the  $Ca_v2.1$  calcium channel, although, in normal conditions, local stimulation should evoke neurotransmitter release at a high probability from the synaptic terminals of the thalamocortical projection. The other possibility was that postsynaptic GABA<sub>A</sub> receptors were reduced in number or their functional properties were altered in *tg* mice. To examine the two possibilities, miniature IPSCs (mIPSCs) were recorded in the presence of CNQX, APV, and TTX (1  $\mu$ M). TTX was used to block voltage-dependent Na<sup>+</sup> channel so that spontaneous firings of neuronal populations were suppressed. Typical traces of mIPSCs in wt and *tg* mice are shown in

Fig. 3A. The cumulative probability distributions of mIPSC amplitudes (Fig. 3B, *right*) and inter-event intervals (IEIs) (Fig. 3B, *left*) showed similar distributions in wt and *tg* mice. The averaged median mIPSC amplitude ( $26.8 \pm 4.3$  pA;  $n = 5$  for wt and  $32.2 \pm 6.2$  pA;  $n = 5$  for *tg*;  $p > 0.05$ ; Fig. 3C, *right*) and the averaged median IEIs ( $12.4 \pm 4.4$  ms;  $n = 5$  for wt and  $14.2 \pm 3.6$  ms;  $n = 5$  for *tg*;  $p > 0.05$ ; Fig. 3C, *left*) showed no significant difference between wt and *tg* mice. These results suggested that the postsynaptic GABA<sub>A</sub> receptors on the layer IV pyramidal cells were intact.

### **Number of inhibitory neurons**

Another possibility to cause the markedly reduced IPSCs in layer IV was that the number of inhibitory interneurons was reduced in layer IV of *tg* mice. To test this possibility distribution of inhibitory neurons was analyzed by the immunohistochemical method using polyclonal antibody against the GABA synthetic enzyme glutamic acid decarboxylase (GAD) (McLaughlin et al., 1975a,b; Ribak et al., 1976). Anti-GAD polyclonal antibody labels not only cell bodies of inhibitory interneurons but also GABAergic nerve terminals surrounding somata of excitatory neurons (Kaufman et al., 1991).

Sections of the barrel cortex were cut in coronal section (40  $\mu$ m). To ascertain the

barrel cortex, I performed Nissle staining on alternate sections. There was no obvious difference in the distribution of GAD-immunoreactive cells in the barrel cortex between wt and *tg* mice (Fig. 4A). Cell bodies of large, presumable pyramidal, neurons in layer IV in both wt and *tg* mice were similarly surrounded by immunoreactive GABAergic terminals (Fig. 4B, indicated by arrows). The density of GAD-immunoreactive cells in layer IV showed no statistical difference between wt ( $184 \pm 26$  cells/mm<sup>2</sup>;  $n = 5$ ) and *tg* mice ( $192 \pm 24$  cells/mm<sup>2</sup>;  $n = 5$ ;  $p > 0.05$ ; Fig. 4C). Together with the intact mIPSCs, these results suggested that the reduced IPSCs in *tg* mice was caused by functional impairments of neurotransmitter release from the presynaptic nerve terminals.

### **Layer-specific impairment of IPSCs**

Thalamocortical afferents form synapses not only with neuronal elements in layer IV including pyramidal cells (White and Hersch, 1981) but also with corticalthalamic pyramidal cells, which are located in lower layer V and upper layer VI and project to the ventrobasal complex of the thalamus (White and Hersch, 1982; White and Killer, 1987). To test whether the impairment IPSCs was dependent on the laminar position in the somatosensory cortex, locally evoked IPSCs and EPSCs were recorded in layer V pyramidal cells. Different from the layer IV neurons, the reduction in IPSC amplitude

was not observed in layer V pyramidal cells in *tg* ( $1,063 \text{ pA} \pm 358 \text{ pA}$ ;  $n = 11$ , 1.0 mA stimulation) compared with that of wt mice ( $1144 \pm 387 \text{ pA}$ ;  $n = 10$ , 1.0 mA stimulation;  $p > 0.05$ , Fig. 5A and C). On the other hand, the EPSC amplitude was moderately reduced in layer V pyramidal cells of *tg* ( $392 \pm 41 \text{ pA}$ ;  $n = 10$ , 10 mA stimulation) compared to that of wt mice ( $736 \pm 157 \text{ pA}$ ;  $n = 10$ , 10 mA stimulation;  $*p < 0.05$ , Fig. 5B and D). The extent of the EPSC reduction in layer V (53%), however, was not as remarkable as the IPSC reduction in layer IV (8%).

### **Developmental changes in IPSCs**

Homozygous *tg* mice develop absence seizures at about 3 weeks of age (Noebels, 1984). If the impairment of IPSCs contributes to the epileptogenesis, the IPSCs may show a related developmental change. To examine this prediction, I studied the developmental effect on the synaptic transmission, by comparing non-epileptic young (P14-16) and epileptic adult (P21-30) *tg* mice.

In younger mice, the amplitude of locally evoked IPSCs in layer IV pyramidal cells was slightly increased in non-epileptic *tg* ( $1,234 \pm 415 \text{ pA}$ ;  $n = 10$ ) compared with wt mice ( $752 \pm 244 \text{ pA}$ ;  $n = 10$ ), but the difference was not statistically significant (1.0 mA stimulation;  $p > 0.05$ ; Fig. 6 A and C). The amplitude of locally evoked IPSCs in layer V

pyramidal cells did not make a difference between wt ( $1,252 \pm 247$  pA;  $n = 10$ ) and non-epileptic *tg* mice ( $1,049 \pm 373$  pA;  $n = 10$ , 1.0 mA stimulation;  $p > 0.05$ ; Fig. 6 B and D). The results suggested that the inhibitory synaptic transmission in layer IV and layer V pyramidal neurons was intact in young non-epileptic *tg* mice.

In both layers IV and V, the EPSC peak amplitudes increased with increments of stimulation intensity in wt and *tg* mice at P14-16 (Fig. 7A and B). The averaged EPSC peak amplitudes of layer IV pyramidal cells ( $333 \pm 81$  pA;  $n = 10$  for *tg* and  $407 \pm 75$  pA;  $n = 10$  for wt;  $p > 0.05$ , 1.0 mA stimulation; Fig. 7 A and C) and of layer V pyramidal cells ( $266 \pm 69$  pA;  $n = 10$ ; for *tg* and  $523 \pm 212$  pA;  $n = 10$ ; for wt,  $p > 0.05$ ; 1.0 mA stimulation; Fig. 7 B and D) were not significantly different between wt and *tg* mice.

During the development period from P14-16 to P21-30, the amplitude of locally evoked IPSCs almost doubled in wt mice, whereas the IPSC amplitude of *tg* mice dramatically diminished in layer IV pyramidal cells (Fig. 2C and Fig. 6C). The IPSC amplitudes in layer V did not show such a developmental change (Fig. 5C and Fig. 6D). The results indicated that the impairment of IPSCs in layer IV was well correlated with the onset of absence seizures.

## **Developmental switching of Ca<sup>2+</sup> channel subtypes**

The previous studies demonstrated that Ca<sup>2+</sup> channels involved in neurotransmitter release switch developmentally from the Ca<sub>v</sub>2.2 (N-type) to Ca<sub>v</sub>2.1 (P/Q-type) Ca<sup>2+</sup> channels at various mammalian fast synapses (Iwasaki et al., 2000). Although the contribution of the Ca<sub>v</sub>2.2 channel to EPSCs in layer IV pyramidal cells of the visual cortex was reported not to change developmentally (Iwasaki et al., 2000), developmental changes in Ca<sup>2+</sup> channel subtypes dependency of cortical IPSCs were not well investigated. Because the developmental subtype switch usually occurs around 2 weeks of age, it was expected that the switching from Ca<sub>v</sub>2.2 to Ca<sub>v</sub>2.1 Ca<sup>2+</sup> channel might lead to the impairment of IPSCs in *tg* mice.

In layer IV pyramidal cells of the somatosensory cortex, I measured developmental changes in sensitivity of IPSCs to the Ca<sub>v</sub>2.1 channel-selective blocker  $\omega$ -Aga-IVA (200 nM) and the Ca<sub>v</sub>2.2 channel-selective blocker  $\omega$ -CgTx-GVIA (3  $\mu$ M). At P14-15, application of  $\omega$ -Aga-IVA to brain slices of wt mice weakly blocked IPSCs (Fig. 8A). Subsequent coapplication of  $\omega$ -CgTx-GVIA almost completely blocked the remaining IPSCs (Fig. 8A). On the other hand, at P21-22, the IPSCs were more strongly reduced by application of  $\omega$ -Aga-IVA (Fig. 8B). The  $\omega$ -Aga-IVA sensitive fraction of IPSCs was increased from  $19 \pm 6\%$  at P14-15 to  $47 \pm 4\%$  at P21-22 ( $n = 5$ ;  $**p < 0.01$ ; Fig. 8C).

These results demonstrated that whereas the  $\text{Ca}_v2.1$  channel plays a minor role in young mice, it plays a predominant role in adult mice for IPSCs in layer IV pyramidal cells of the somatosensory cortex. Developmental switching of  $\text{Ca}^{2+}$  channel subtypes in *tg* mice thus leads to reduction in  $\text{Ca}^{2+}$  influx into nerve terminals, consequently impairing synaptic transmission.

### **Propagation of neuronal excitability**

To investigate the effects on cortical excitability of the impaired IPSCs in layer IV pyramidal neurons of epileptic *tg* mice, I examined spatial propagation of neuronal excitability using a 64-channel field potential recording system (MED64 system).

There have been already some published works that reported measurements of field potentials using the multi-channel recording system, but the interpretation of the responses to local stimulation are conflicting (Shimono et al., 2000; Wirth and Lüscher, 2004). Therefore, first, I made a pharmacological analysis of the synaptic local field potentials (sLFP), and determined which components of the recordings corresponded to the excitatory or inhibitory components (Fig. 9). Fig. 9A shows a recording site on the thalamocortical slice. An extra stimulation electrode was placed within a barrel, and the evoked field potentials at the 64 sites were recorded simultaneously (Fig. 9B).

Following the stimulation, a negative (downward) component appeared mainly around the stimulation site in layer IV (Fig. 9B and C). This negative component of sLFP was almost completely abolished after blocking the synaptic transmission with perfusion of a  $\text{Co}^{2+}$ -containing ACSF (where  $\text{Ca}^{2+}$  was replaced with 5mM  $\text{Co}^{2+}$ , Fig. 9D). The remaining component after  $\text{Co}^{2+}$  application probably corresponds to a fiber volley or axon terminal potential (Swadlow and Gusev, 2000) evoked by direct stimulation of the axons. The negative sLFP component in layer IV was further dissected pharmacologically. The negative component was almost completely abolished by application of CNQX and APV, indicating that this component essentially corresponded to the excitatory component (Fig. 9F). Application of picrotoxin (50  $\mu\text{M}$ ), however, led to a slight increase in peak amplitude of the negative component, suggesting that the negative component also contained a minor inhibitory component, but it was much smaller than the excitatory component (Fig. 9E). The negative component in the presence of picrotoxin was blocked by CNQX (10  $\mu\text{M}$ ) and APV (100  $\mu\text{M}$ ) (Fig. 9E). A small negative component remained after application of both CNQX and APV. This was likely evoked by direct stimulation of fibers (Fig. 9E and F). These observations indicated that the negative sLFP component in layer IV mainly corresponded to local excitatory postsynaptic potentials. In order to analyze laminar and columnar activity

profiles, I calculated the average of the negative sLFP components along the horizontal and vertical axes of the cerebral cortex .

The spatial propagation of the negative sLFP component was visualized using pseudocolor imaging, and compared between wt and *tg* mice (P21-30). The time interval from the stimulus onset to the peak of the activation of single barrels varied considerably between wt and *tg* mice (Fig. 10A). The excitation initiated in a barrel also spread more widely in the horizontal directions in *tg* more than in wt mice. So the horizontal propagation beyond the stimulated barrel was analyzed by measuring sLFP amplitude along the layer IV at the time when the response at the stimulus location was the maximum. The sLFP amplitude at the horizontal distance of 100  $\mu\text{m}$  away from the stimulus location was normalized to that at the stimulus location, and plotted against the increment of stimulus intensity (Fig. 10B). The normalized sLFP amplitude at 100  $\mu\text{m}$  was clearly increased in *tg* than in wt mice with +50  $\mu\text{A}$  (above the minimum stimulation) and stronger stimulations ( $0.72 \pm 0.08$ ;  $n = 10$  for *tg* and  $0.36 \pm 0.09$ ;  $n = 10$  for wt, +200  $\mu\text{A}$  stimulation  $**p < 0.01$ ; Fig. 10B and C). The normalized sLFP amplitudes at locations more distant than 100  $\mu\text{m}$  from the stimulus location were not different between wt and *tg* mice with +200  $\mu\text{A}$  stimulation (above the minimum stimulation) (Fig. 10C). This clearly demonstrated that the spatial activity in *tg* mice

spread horizontally within a stimulated barrel. Spreading of the excitatory signals in the vertical directions made no statistical difference between *tg* and wt mice ( $0.75 \pm 0.06$ ;  $n = 10$  for *tg* and  $0.59 \pm 0.07$ ;  $n = 10$  for wt,  $p > 0.05$ ; 100  $\mu\text{m}$  from the stimulus location).

In layer V, the normalized sLFP amplitudes at 100  $\mu\text{m}$  from the stimulus location were not different between wt and *tg* mice ( $0.23 \pm 0.23$ ,  $n = 3$  in *tg* and  $0.24 \pm 0.13$ ,  $n = 6$ , in wt,  $p > 0.05$ ) with +200  $\mu\text{A}$  stimulation (data not shown).

Current-source density (CSD) analysis was also tried, but it failed to give consistent results, probably because the recorded responses were too small and because the cellular architecture of the barrel cortex was not so organized as the hippocampus and other areas.

### **Developmental change in neuronal excitability**

To examine whether the change in spreading of excitatory activity in *tg* mice was related to development and seizure, I measured spatial propagation of the negative sLFP component in P14-16 wt and non-epileptic *tg* mice (Fig. 11A). The normalized sLFP amplitude at the horizontal distance of 100  $\mu\text{m}$  away from stimulus location was not different between wt and non-epileptic *tg* mice with various stimulus intensities tested ( $0.45 \pm 0.12$ ;  $n = 10$  for *tg* and  $0.40 \pm 0.14$ ;  $n = 10$  for wt,  $p > 0.05$ ; Fig. 11B and C).

The normalized sLFP amplitudes at locations at further horizontal distances from the stimulus location were not statistically different between wt and *tg* mice (Fig. 11C).

These results, gathered together, suggested that the impaired layer IV IPSCs lead to increased spatial activity in the horizontal directions within the stimulated barrel and the adjacent area of 200  $\mu\text{m}$  in epileptic *tg* mice.

## **Discussion**

Absence epilepsy has long been speculated to arise from an aberration of the interplay between the cerebral cortex and the thalamus. Despite extensive studies for several decades, the interactions between the cerebral cortex and the thalamus at the onset of the seizure activity and during it are yet poorly understood at the synaptic level. Among the seizure models with single gene mutations, *tg* mice are one of the most famous and the most extensively studied (Burgess and Noebels, 1999), but little is known about synaptic transmission in the cerebral cortex of *tg* mice. In this study, I studied excitatory and inhibitory synaptic transmissions within the layer IV of the somatosensory cortex in epileptic *tg* mice.

### **Absence epilepsy in *tg* mice**

Much of present knowledge of the underlying etiology of human absence epilepsy has benefited greatly from a use of appropriate animal models. Validation of animal models of absence epilepsy requires certain criteria to be met for them to be representative of the human condition (see review Snead, 1995). The criteria include (1) bilaterally synchronous spike wave discharges associated with behavioral arrest  $\pm$  head drops, and nystagmus, (2) attenuation or block by ethosuximide, and (3) spike and wave discharges

originating in thalamus and/or cortex. Fortunately, mouse absence models harboring single gene mutations frequently satisfy these criteria, and therefore the models are particularly amenable to the genetic analysis. The identification of the gene mutation sites has greatly facilitated experimental analyses of the basic pathophysiological mechanisms of epilepsy, and provided valuable candidate genes for testing in humans.

Among these seizure models with single gene mutations, particularly among those associated with defects in genes encoding subunits of voltage-gated  $\text{Ca}^{2+}$  channels, *tg* mice are the most famous and have been most extensively studied (Burgess and Noebels, 1999). Despite the long history of the *tg* research, however, little is known about synaptic transmission in the cerebral cortex of *tg* mice. It is evident that the mechanisms by which mutant  $\text{Ca}^{2+}$  channel genes lead to the absence epilepsy phenotype is certainly complicated and its elucidation will be a difficult task. Here, to reveal the network mechanism for epilepsy caused by a  $\text{Ca}^{2+}$  channel mutation, I examined excitatory and inhibitory synaptic responses in thalamocortical slice preparations from epileptic *tg* mice.

#### **Layer IV inhibitory synapses dysfunction in epileptic *tg* mice**

The principal finding of this study was a significant reduction (~90%) in the amplitude

of IPSCs, but not of EPSCs, in layer IV pyramidal cells of epileptic *tg* mice (Fig. 2).

Similar results were obtained with the thalamocortical responses (Fig. 1).

In the present work, immunohistochemical study showed that there were no significant differences in the number of GAD-immunoreactive cells in layer IV between wt and *tg* mice (Fig. 5). GAD-positive terminals were observed around large somata of neurons similarly in wt and *tg* mice. Analyses of mIPSCs recorded in layer IV pyramidal cells demonstrated no difference in amplitude or in inter-event interval between wt and *tg* mice. All these results suggest that significant decrease of layer IV IPSCs was caused by dysfunction of neurotransmitter release from presynaptic terminals in these inhibitory synapses (Fig. 3). Because neurotransmitter release is dependent on calcium influx and the relationship is non-linear, it is possible that a moderate reduction in calcium influx by a Ca<sup>2+</sup> channel mutation severely decrease neurotransmitter release in some of the synapses.

### **Dysfunction of inhibitory synapses is layer-specific**

Because the Ca<sub>v</sub>2.1 channel is the predominant Ca<sup>2+</sup> channel type in the central nervous system, it is rather surprising that the neurological dysfunctions are relatively confined to specific neuronal populations. The reduction in IPSCs was prominent in layer IV, but it was not observed in layer V in *tg* mice. Moreover, EPSCs were largely intact in the

examined synapses, although the EPSCs amplitude was mildly reduced in layer V. These results demonstrate that the synaptic dysfunction is critically dependent on cellular types (Fig. 4).

Previous studies suggested that several factors contribute to determining the severity of impairments of synaptic transmission caused by mutations. The study of synaptic transmission in the cerebellar cortex of *tg* mice showed that the parallel fiber-Purkinje cell synapses were severely impaired, whereas the climbing fiber-Purkinje cell synapses were surprisingly intact (Matsushita et al., 2002). Because the parallel fiber-Purkinje cell synapses and the climbing fiber-Purkinje cell synapses are low- and high-release probability synapses, respectively, this result suggested that low-release probability synapses are more vulnerable to the mutational effect.

Another important factor is compensatory mechanisms to restore the impairment of inhibitory synaptic transmission. When the  $Ca_v2.1$  (P/Q-type) channel is defective in *tg* mice, other types of  $Ca^{2+}$  channel, such as the  $Ca_v2.2$  (N-type) and  $Ca_v2.3$  (R-type) channels, are expected to compensate the mutational effects. But it appears that different neuronal populations show different flexibility for the compensatory mechanism. For example, the  $Ca_v2.2$ -deficient mice show surprisingly normal development and normal behaviors. Careful investigation showed that they have an abnormal baroreceptor reflex,

which is mediated by the sympathetic nervous system (Ino et al., 2001).

Electrophysiological measurement from neurons of the superior cervical ganglion showed the function of these  $Ca_v2.2$  channel-dependent neurons were not restored by other types of calcium channels. Thus, I speculate that some neuronal populations are more dependent on a particular type of calcium channels than others, and functions of such neurons are more easily impaired in mutant brains. In support of this notion, the previous report demonstrated that hippocampal inhibitory interneurons have preference for  $Ca_v2.1$  or  $Ca_v2.2$  channel (Poncer et al., 1997). Hippocampal inhibitory neurons in stratum lucidum and stratum oriens use only the  $Ca_v2.1$  channel, whereas other interneurons are purely dependent on the  $Ca_v2.2$  channel. In this context, the observation that the IPSCs in layer IV become more dependent on the  $Ca_v2.1$  channel supports the notion that the inhibitory interneurons in layer IV in *tg* mice are less flexible than other neurons that other types of calcium channels cannot compensate the mutational effect.

### **Types and functions of layer IV interneurons**

Neurons in the cortical layer IV receive synaptic inputs from the thalamus and from neighboring neurons in layer IV (Hubel and Wiesel, 1962; McGuire et al., 1984; for

review see Sherman and Guillery, 1996). The present work suggested a critical role of layer IV inhibitory interneurons for absence seizure. Previous studies showed that inhibitory interneurons in layers IV that are activated by the thalamocortical projections are morphologically heterogeneous in terms of their dendrites and axons (Porter et al., 2001; Amitai et al., 2002). Within this heterogeneity, however, there is a clear grouping of cells into several distinct morphological types, which differ in the vertical and horizontal distributions of their axons, and thereby in their potential role in the thalamocortical circuit.

In previous studies, inhibitory interneurons in the cerebral cortex are often grouped into two types of interneurons based on the patterns of the intrinsic firing, which are the fast-spiking (FS) cells and the low-threshold-spiking (LTS) cells (Cauli et al., 1997; Kawaguchi and Kubota, 1997; Guta et al., 2000). Inputs from thalamocortical relay cells were more selective for FS cells, and frequently and strongly excite them (Agmon and Connors, 1991; Porter et al., 2001; Beierlein et al., 2002), whereas the thalamocortical inputs only rarely and weakly excite LTS cells (Gibson et al., 1999; Beierlein et al., 2000). These results suggest that FS neurons play a dominant role in feedforward inhibition of the thalamocortical projection.

The present study indicated that the thalamocortical feedforward inhibition was

profoundly dysfunctional in epileptic *tg* mice. Considering the previous studies that the thalamocortical feedforward inhibition is mediated *via* FS cells, it is speculated that dysfunction of the feedforward inhibition in *tg* mice is because of dysfunction in FS cell-mediated pathway.

### **Development-dependent dysfunction of inhibitory synapses**

Absence seizure in *tg* mice begins at about 3 weeks of age (Noebels, 1984). The IPSC amplitude in layer IV pyramidal cells was reduced in epileptic adult *tg* mice, but not in non-epileptic young *tg* mice (Fig. 6). This result indicates that the inhibitory synapses become functional in the early developmental stages, but they lose their function later. These findings imply a close relationship between impaired IPSC and absence epilepsy.

The Ca<sup>2+</sup> channel involved in neurotransmitter release often switches developmentally from the Ca<sub>v</sub>2.2 (N-type) channel to the Ca<sub>v</sub>2.1 (P/Q-type) channel at various mammalian fast synapses (Iwasaki et al., 2000). The contribution of the Ca<sub>v</sub>2.2 channel is decreased during postnatal development in cerebellar and thalamic inhibitory synapses, auditory brainstem excitatory synapses (Iwasaki and Takahashi, 1998), and neuromuscular junctions (Rosato Siri and Uchitel, 1999). However, EPSCs in layer IV of the visual cortex remain dependent on the Ca<sub>v</sub>2.2 channel throughout the postnatal development (Iwasaki et al., 2000).

In the present work, the sensitivity of inhibitory synaptic transmission to  $\omega$ -AgaIVA increased developmentally in layer IV, indicating the subtype switching (Fig. 8). Because the timing of subtype switching and the onset of seizure coincide, I speculate that, through the subtype switching, compensational effects by the  $Ca_v2.2$  channel and others are lost and the impairment of synaptic transmission becomes overt, leading to disruption of well-balanced excitatory and inhibitory networks.

### **Propagation of neuronal excitability in epileptic *tg* mice**

In the barrel somatosensory cortex of rodents, layer IV neurons are arranged in discrete barrels. (Woolsey and Van der Loos, 1970). It has been thought that GABAergic interneurons of the cerebral cortex are actively involved in controlling cerebral excitability (Jones, 1993). The previous studies with voltage sensitive dyes and multi-electrode arrays showed that the functional confinement of the spatiotemporal excitation to a single barrel is controlled by GABAergic inhibition (Petersen and Sakmann, 2001; Laaris and Keller, 2002; Wirth and Lüscher, 2004). A small-spot stimulation at the center of a barrel generates an excitation in a restricted area within the single barrel. Even after blocking inhibitory synaptic responses, the excitatory signal in the barrels was limited to the barrel border (Petersen and Sakmann, 2001). In this study,

using a 64-channel field potential recording system, I showed that the spatial propagation of neuronal excitability evoked by stimulation at the center of a barrel is increased in the horizontal directions in epileptic *tg* mice (Fig. 10), but non-epileptic *tg* mice (Fig. 11). It is notable that the spread width of  $\sim 200 \mu\text{m}$  in epileptic *tg* mice is similar to the barrel width of  $\sim 200 \mu\text{m}$ . The results suggested that increased spatial activity in epileptic *tg* mice was caused by the dysfunction of GABAergic inhibition, but the increased spatial activity remained restricted inside the barrel.

### **Functional implication**

Absence seizure is neurophysiologically, pharmacologically, and developmentally unique. A number of animal models of generalized absence seizure and sophisticated techniques of EEG recording, which allow investigation of cortical and thalamic networks, have begun to understand the pathophysiological mechanisms of this disorder. The basic underlying mechanism appears to involve the thalamocortical circuitry and the generation of abnormal oscillatory rhythm from that particular neuronal network. Although based on the decades-old hypothesis that an imbalance between excitation and inhibition within the thalamocortical loop might be critical for the genesis of absence seizure (Gillor et al., 1990; for review, see Manning, 2003), the present studies have

clearly identified, for the first time, an exact location of drastically impaired inhibitory synaptic transmission in *tg* mice. The present results suggest that the cortical inhibitory synapses are critically involved in generation of absence seizure.

Previous studies demonstrate the relative importance of the cortical component of the thalamocortical circuitry on SWDs activity (Avoli and Gloor, 1982; Gloor and Fariello, 1988). More recent studies imply that cortical component is important in the initiation of SWDs (Seidenbecher et al., 1998; D’Arcangel et al., 2002). In fact investigation of seizure activity has been shown to persist by means of thalamectomy, indicating a principal role for the cortex in the initiation of SWDs activity (Steriade and Contreras, 1998), although the thalamus is required to maintain rhythmicity once the seizure is established (D’Arcangel et al., 2002).

It is speculated that, once layer IV principal neurons receive strong or repeated thalamocortical inputs, the regulatory failure of the feedforward inhibition caused by dysfunction of inhibitory synapses leads to excessive cortical neuronal excitability and subsequently causes SWDs.

An obvious question is the thalamocortical feedforward inhibition in other model animals of absence seizure. The dysfunction of feedforward inhibition may be common, or alternatively a different aberration of neuronal network may be essential. Further

experiments to characterize the thalamocortical network using other model animals would answer this question. I hope that the results forthcoming may facilitate the development of new approach in the treatment of patients with absence epilepsy.

## References

- Agmon A, Connors BW (1991) Thalamocortical responses of mouse somatosensory (barrel) cortex *in vitro*. *Neuroscience* 41: 365-379.
- Amitai Y, Gibson JR, Beierlein M, Patrick SL, Ho AM, Connors BW, Golomb D (2002) The spatial dimensions of electrically coupled networks of interneurons in the neocortex. *J Neurosci* 22: 4142-4152.
- Avoli M, Gloor P (1982) Interaction of cortex and thalamus in spike and wave discharges of feline generalized penicillin epilepsy. *Exp Neurol* 76: 196-217.
- Avanzini G, Panzica F, de Curtis M (2000) The role of the thalamus in vigilance and epileptogenic mechanism. *Clin Neurophysiol* 111 suppl 2: S19-S26.
- Beierlein M, Fall CP, Rinzel J, Yuste R (2002) Thalamocortical bursts trigger recurrent activity in neocortical networks: layer 4 as a frequency-dependent gate. *J Neurosci* 22: 9885-9894.
- Beierlein M, Gibson JR, Connors BW (2000) A network of electrically coupled interneurons drives synchronized inhibition in neocortex. *Nat Neurosci* 3: 904-910.
- Brecht M, Sakmann B (2002) Dynamic representation of whisker deflection by synaptic potentials in spiny stellate and pyramidal cells in the barrels and septa of layer 4 rat somatosensory cortex. *J Physiol* 543: 49-70.
- Burgess DL, Noebels JL (1999) Single gene defects in mice: the role of voltage-dependent calcium channels in absence models. *Epilepsy Res* 36: 111-122.
- Buzsaki G (1991) The thalamic clock: emergent network properties. *Neuroscience* 41: 351-364
- Cauli B, Audinat E, Lambolez B, Angulo MC, Ropert N, Tsuzuki K, Hestrin S, Rossier J (1997) Molecular and physiological diversity of cortical nonpyramidal cells. *J Neurosci* 17: 3894-3906.

Chiaia NL, Rhoades RW, Bennett-Clarke CA, Fish SE, Killackey HP (1991a) Thalamic processing of vibrissal information in the rat. I. Afferent input to the medial ventral posterior and posterior nuclei. *J Comp Neurol* 314: 201-216.

Chiaia NL, Rhoades RW, Fish SE, Killackey HP (1991b) Thalamic processing of vibrissal information in the rat: II. Morphological and functional properties of medial ventral posterior nucleus and posterior nucleus neurons. *J Comp Neurol* 314: 217-236.

D'Arcangel G, D'Antuono M, Biagini G, Warren R, Tancredi V, Avoli M (2002) Thalamocortical oscillations in genetic model of absence seizures. *Eur J Neurosci* 16: 2383-2393.

Fletcher CF, Lutz CM, O'Sullivan TN, Shaughnessy JD Jr, Hawkes R, Frankel WN, Copeland NG, Jenkins NA (1996) Absence epilepsy in tottering mutant mice is associated with calcium channel defects. *Cell* 87: 607-617.

Gibson JR, Beierlein M, Connors BW (1999) Two networks of electrically coupled inhibitory neurons in neocortex. *Nature* 402: 75-79.

Gloor P, Avoli M, Kostopoulos G (1990) Thalamocortical relationship in generalized epilepsy with bilateral synchronous spike and wave discharges. *Generalized epilepsy, Neurobiological Approaches*, Boston, Birkhauser: pp 190-212.

Gloor P, Fariello RG (1988) Generalized epilepsy: some of its cellular mechanisms differ from those of focal epilepsy. *Trends Neurosci* 11: 63-68.

Gupta A, Wang Y, Markram H (2000) Organizing principles for a diversity of GABAergic interneurons and synapses in the neocortex. *Science* 287: 273-278.

Hubel DH, Wiesel TN (1962) Receptive fields, binocular interaction and functional architecture in the cat's visual cortex. *J Physiol* 160: 106-154.

Ino M, Yoshinaga T, Wakamori M, Miyamoto N, Takahashi E, Sonoda J, Kagaya T, Oki T, Nagasu T, Nishizawa Y, Tanaka I, Imoto K, Aizawa S, Koch S, Schwartz A, Niidome T, Sawada K, Mori Y (2001) Functional disorders of the sympathetic nervous system in mice lacking the  $\alpha_{1B}$  subunit ( $Ca_v$  2.2) of N-type calcium channels. *Proc Natl Acad Sci* 98: 5323-5328.

Iwasaki S, Takahashi T (1998) Development changes in calcium channel types mediating synaptic transmission in rat auditory brainstem. *J physiol* 509: 419-423.

Iwasaki S, Momiyama A, Uchitel OD, Takahashi T (2000) Development changes in calcium channel types mediating central synaptic transmission. *J Neurosci* 20: 59-65.

Jones EG (1993) GABAergic neurons and their role in cortical plasticity in primates. *Cereb Cortex* 3: 361-372 .

Kaufman DL, Houser CR, Tobin AJ (1991) Two forms of the gamma-aminobutyric acid synthetic enzyme glutamate decarboxylase have distinct intraneuronal distributions and cofactor interactions. *J Neurochem* 56: 720-723.

Kawaguchi Y, Kubota Y (1997) GABAergic cell subtypes and their synaptic connections in rat frontal cortex. *Cereb Cortex* 7: 476-486.

Laaris N, Keller A (2002) Functional independence of layer IV barrels. *J Neurophysiol* 87: 1028-1034.

Manning JP, Richards DA, Bowery NG (2003) Pharmacology of absence epilepsy. *Trends Pharmacol Sci* 24: 542-549.

Matsushita K, Wakamori M, Rhyu IJ, Arai T, Oda S, Mori Y, Imoto K (2002) Bidirectional alterations in cerebellar synaptic transmission of *tottering* and *rolling*  $Ca^{2+}$  channel mutant mice. *J Neurosci* 22: 4388-4398.

McCormick DA, Bal T (1997) Sleep and arousal: thalamocortical mechanisms. *Annu Rev Neurosci* 20: 185-215.

McGuire BA, Hornung JP, Gilbert CD, Wiesel TN (1984) Patterns of synaptic input to layer 4 of cat striate cortex. *J Neurosci* 12: 3021-3033.

McLaughlin BJ, Wood JG, Saito K, Roberts E, Wu JY (1975a) The fine structural localization of glutamate decarboxylase in developing axonal processes and presynaptic terminals of rodent cerebellum. *Brain Res* 85: 355-371.

McLaughlin BJ, Baber R, Saito K, Roberts E, Wu JY (1975b) Immunocytochemical localization of glutamate decarboxylase in rat spinal cord. *J Comp Neurol* 164: 305-321.

Meeren HK, Pijn JP, Van Luijckelaar EL, Coenen AM, Lopes da Silva FH (2002) Cortical focus drives widespread corticothalamic networks during spontaneous absence seizures in rats. *J Neurosci* 22: 1480-1495.

Mori Y, Friedrich T, Kim MS, Mikami A, Nakai J, Ruth P, Bosse E, Hofmann F, Flockerzi V, Furuichi T, Mikoshiba K, Imoto K, Tanabe T, Numa S (1991) Primary structure and functional expression from complementary DNA of a brain calcium channel. *Nature* 350: 398-402.

Mori Y, Wakamori M, Oda S, Fletcher CF, Sekiguchi N, Mori E, Copeland NG, Jenkins NA, Matsushita K, Matsuyama Z, Imoto K (2000) Reduced voltage sensitivity of activation of P/Q-type  $Ca^{2+}$  channels is associated with the ataxic mouse mutation *rolling Nagoya* (*tg<sup>rol</sup>*). *J Neurosci* 20: 5654-5662.

Noebels JL (1984) A single gene error of noradrenergic axon growth synchronizes central neurons. *Nature* 310: 409-411.

Noebels JL, Sidman RL (1979) Inherited epilepsy: spike-wave and focal motor seizures in the mutant mouse tottering. *Science* 204: 1334-1336.

Oka H, Shimono K, Ogawa R, Sugihara H, Taketani M (1999) A new planar multielectrode array for extracellular recording: application to hippocampal acute slice. *J Neurosci Methods* 93: 61-67.

Petersen CC, Sakmann B (2001) Functionally independent columns of rat somatosensory barrel cortex revealed with voltage-sensitive dye imaging. *J Neurosci* 21: 8435-8446.

Poncer JC, McKinney RA, Gähwiler BH, Thompson SM (1997) Either N- or P-type calcium channels mediate GABA release at distinct hippocampal inhibitory synapses. *Neuron* 18: 463-472.

Porter JT, Johnson CK, Agmon A (2001) Diverse types of interneurons generate thalamus-evoked feedforward inhibition in the mouse barrel cortex. *J Neurosci* 21: 2699-2710.

Randall A, Tsien RW (1995) Pharmacological dissection of multiple types of Ca<sup>2+</sup> channel currents in rat cerebellar granule neurons. *J Neurosci* 15: 2995-3012.

Ribak CE, Vaughn JE, Saito K, Barber R, Roberts E (1976) Immunocytochemical localization of glutamate decarboxylase in rat substantia nigra. *Brain Res* 116: 287-298.

Rosato Siri MD, Uchitel OD (1999) Calcium channels coupled to neurotransmitter release at neonatal rat neuromuscular junctions. *J Physiol* 514: 533-540.

Sather WA, Tanabe T, Zhang JF, Mori Y, Adams ME, Tsien RW (1993) Distinctive biophysical and pharmacological properties of class A (BI) calcium channel alpha 1 subunits. *Neuron* 11: 291-303.

Schubert D, Kötter R, Zilles K, Luhmann HJ, Staiger JF (2003) Cell type-specific circuits of cortical layer IV spiny neurons. *J Neurosci* 23: 2961-2970.

Seidenbecher T, Staak R, Pape HC (1998) Relations between cortical and thalamic cellular activities during absence seizure in rats. *Eur J Neurosci* 10: 1103-1112.

Sherman SM, Guillery RW (1996) Functional organization of thalamocortical relays. *J Neurophysiol* 76: 1367-1395.

Shimono K, Brucher F, Granger R, Lynch G, Taketani M (2000) Origins and distribution of cholinergically induced  $\beta$  rhythms in hippocampal slices. *J Neurosci* 20: 8462-8473.

Simons DJ, Woolsey TA (1984) Morphology of Golgi-Cox-impregnated barrel neurons in rat SmI cortex. *J Comp Neurol* 230:119-132.

Snead OC 3rd (1995) Basic mechanisms of generalized absence seizures. *Ann Neurol* 37: 146-157.

Starr TV, Prystay W, Snutch TP (1991) Primary structure of a calcium channel that is highly expressed in the rat cerebellum. *Proc Natl Acad Sci USA* 88: 5621-5625.

Stea A, Tomlinson WJ, Soong TW, Bourinet E, Dubel SJ, Vincent SR, Snutch TP (1994) Localization and functional properties of a rat brain  $\alpha_{1A}$  calcium channel reflect similarities to neuronal Q- and P-type channels. *Proc Natl Acad Sci USA* 91: 10576-10580.

Steriade M, Contreras D (1998) Spike-wave complexes and fast components of cortically generated seizures. I. Role of neocortex and thalamus. *J Neurophysiol* 80: 1439-1455.

Swadlow HA, Gusev AG (2000) The influence of single VB thalamocortical impulses on barrel columns of rabbit somatosensory cortex. *J Neurophysiol* 83: 2802-2813.

Wakamori M, Yamazaki K, Matsunodaira H, Teramoto T, Tanaka I, Niidome T, Sawada K, Nishizawa Y, Sekiguchi N, Mori E, Mori Y, Imoto K (1998) Single tottering mutations responsible for the neuropathic phenotype of the P-type calcium channel. *J Biol Chem* 273: 34857-34867.

White EL, Hersch SM (1981) Thalamocortical synapses of pyramidal cells which project from SmI to MsI cortex in the mouse. *J Comp Neurol* 198: 167-181.

White EL, Hersch SM (1982) A quantitative study of thalamocortical and other synapses involving the apical dendrites of corticothalamic projection cells in mouse SmI cortex. *J Neurocytol* 11: 137-157.

White EL, Keller A (1987) Intrinsic circuitry involving the local axon collaterals of corticothalamic projection cells in mouse SmI cortex. *J Comp Neurol* 262: 13-26.

Williams D (1953) A study of thalamic and cortical rhythms in *petit mal*. Brain 76: 50-69.

Wirth C, Lüscher HR (2004) Spatiotemporal evolution of excitation and inhibition in the rat barrel cortex investigated with multielectrode arrays. J Neurophysiol 91: 1635-1647.

Woolsey TA, Van der Loos H (1970) The structural organization of layer IV in the somatosensory region (SI) of mouse cerebral cortex. The description of a cortical field composed of discrete cytoarchitectonic units. Brain Res 17: 205-242.

Zhang JF, Randall AD, Ellinor PT, Horne WA, Sather WA, Tanabe T, Schwarz TL, Tsien RW (1993) Distinctive pharmacology and kinetics of cloned neuronal  $Ca^{2+}$  channels and their possible counterparts in mammalian CNS neurons. Neuropharmacology 32: 1075-1088.

## **Acknowledgments**

I would like to express my sincere appreciation to Dr. Keiji Imoto, Dr. Mariko Miyata, Dr. Tsuyoshi Inoue, and Dr. Satake Shin'ichiro, for their generous support and valuable guidance through this study. I am also sincerely grateful to Dr. Yasuo Kawaguchi for his helpful discussion and advice of histological procedure, and Dr. Ken Shimono for his technical advice of MED64 system. I would like to Mrs. Miki Yoshitomo and Mrs. Naomi Fukuta for their excellent technical assistance. I wish to thank all the member of Division of Neural Signaling for the support and kindness.

**Fig.1. Thalamocortical IPSC and EPSC recorded from layer IV pyramidal cells.**

The thalamic stimulation elicited EPSC and IPSC in layer IV pyramidal cells of somatosensory cortex in wt and *tg* mice (P21-30).

A. A thalamocortical brain slice preparation is shown by a cytochrome c oxidase staining. Scale bar 1mm. The marker (*black*) indicates a typical position of stimulation. A barrel is indicated by a dotted circle. Recordings were made from neurons in a barrel. VB, ventrobasal nucleus of the thalamus; IC, internal capsule.

B. A morphologically identified pyramidal cell labeled with biocytin. Counter staining with methylgreen. Scale bar is 100  $\mu\text{m}$ .

C. Synaptic currents evoked by thalamic stimulation were recorded from a layer IV pyramidal cell in wt mice. EPSC was recorded with a holding potential of -60 mV (*upper trace*). When the holding potential was 0 mV, IPSC became prominent (*lower trace*). In the recorded cells, mean values for the holding current ( $98.2 \pm 14.7$  pA;  $n = 12$  for wt;  $103.1 \pm 23.9$  pA,  $n = 11$  for *tg*;  $p > 0.05$ ) and the serial resistance ( $13.0 \pm 0.77$  M $\Omega$ ;  $n = 12$  for wt;  $11.8 \pm 0.89$  M $\Omega$ ;  $n = 11$  for *tg*;  $p > 0.05$ ) did not significantly differ between wt and *tg* mice.

D. EPSC (*upper trace*) and IPSC (*lower trace*) in *tg* mice. The amplitude of IPSC was smaller compared to that of EPSC. Calibration scales are common to C and D.

E. The relationship between the IPSC amplitude and the EPSC amplitude. Each point represents data from one neuron. Lines show linear least-square fit for wt and *tg* mice.

F. The comparison of the IPSC/EPSC ratio. The IPSC/EPSC ratio was greatly decreased in *tg* compared with wt mice. The data represent the means  $\pm$  SEMs.  $**p < 0.01$ .

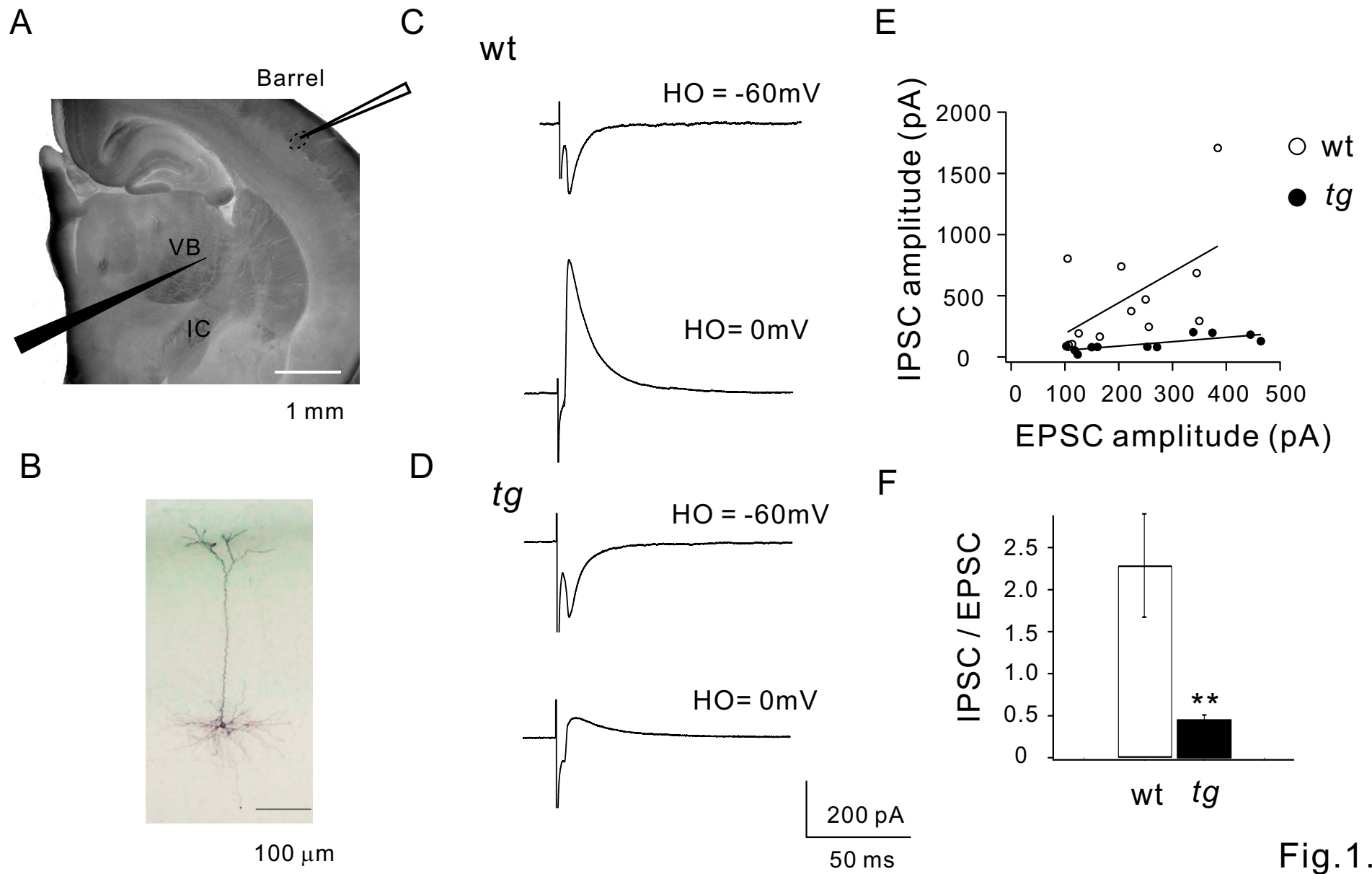


Fig.1.

**Fig.2. Impaired IPSCs of layer IV pyramidal cells in *tg* mice (P21-30)**

IPSCs and EPSCs were evoked by local stimulation in layer IV pyramidal cells of the barrel cortex in wt and *tg* mice at P21-30.

A. IPSCs were recorded in the presence of CNQX (10  $\mu$ M) and APV (100  $\mu$ M). In the recorded cells, mean values for the holding current ( $146.9 \pm 25.3$  pA;  $n = 11$  for wt;  $175.8 \pm 50.4$  pA;  $n = 12$  for *tg*;  $p > 0.05$ ) and the serial resistance ( $13.7 \pm 0.62$  M $\Omega$ ;  $n = 11$  for wt;  $13.1 \pm 0.86$  M $\Omega$ ;  $n = 12$  for *tg*;  $p > 0.05$ ) did not significantly differ between wt and *tg* mice. Typical IPSC traces evoked by 1.0 mA stimulation (average of five recordings) (*top*). A expanded trace is also shown for *tg* (*top right*). The IPSC peak amplitude was plotted against the intensity of stimulation for wt and *tg* mice. In *tg* mice, the IPSC amplitude was significantly smaller, and remained suppressed even if the stimulus intensity was increased up to 10 mA (*bottom*).

B. EPSCs were recorded in the presence of bicuculline (10  $\mu$ M). Typical EPSCs traces evoked by 10 mA stimulation (average of five recordings) (*right*). The EPSCs amplitude increased with increment of stimulation intensity in both wt and *tg* mice (*left*).

C, D. Averaged IPSC peak amplitudes with stimulation intensity of 1.0 mA (C) and averaged EPSC peak amplitudes with stimulation intensity of 10 mA (D). The IPSC amplitude was significantly reduced (~90%) in *tg* mice. However, the EPSC amplitudes of *tg* was not significantly different from that of wt mice. The data represent the means  $\pm$  SEMs.  $**p < 0.01$ .

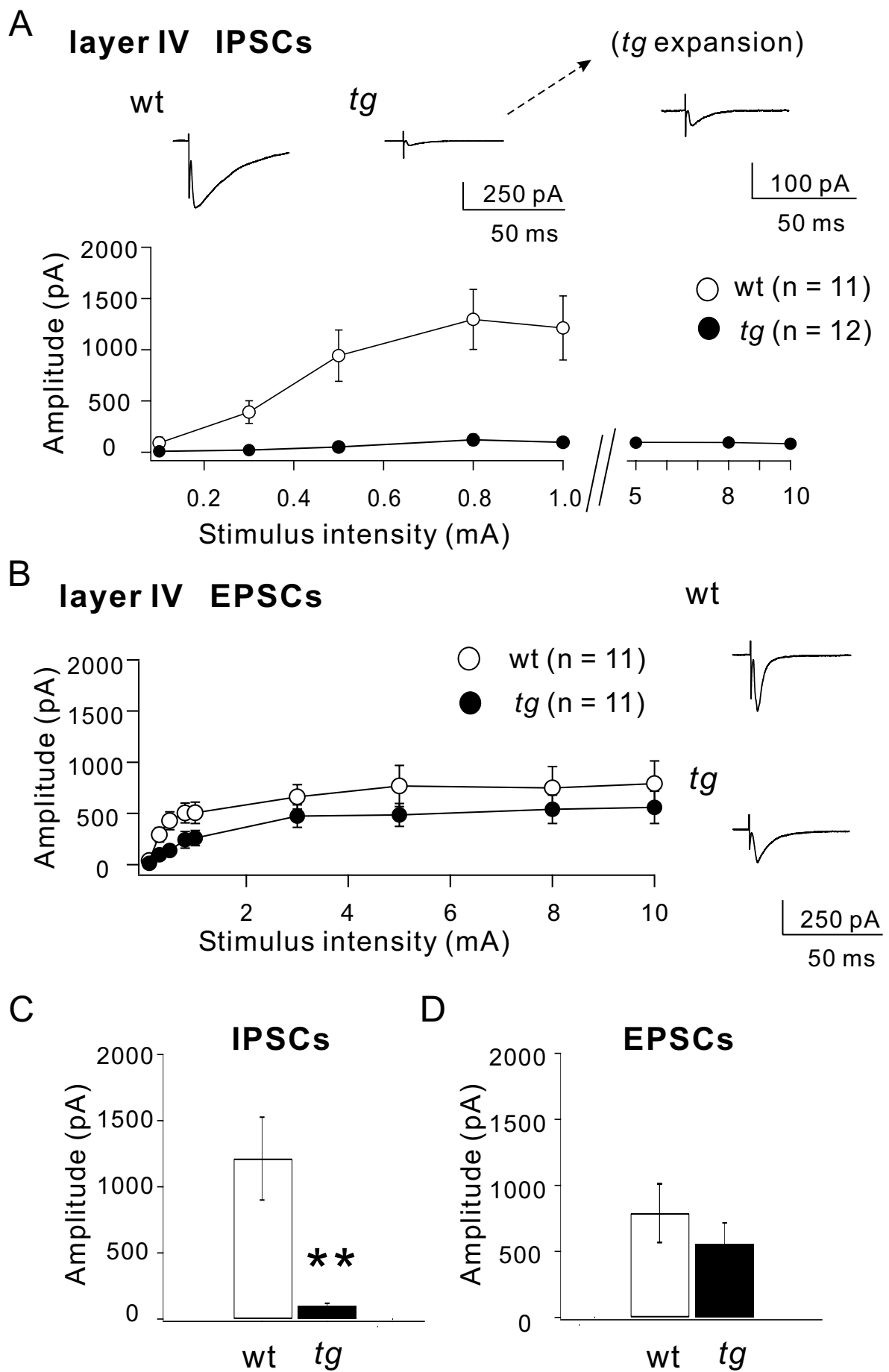


Fig.2.

**Fig.3. mIPSCs in layer IV pyramidal cells in wt and *tg* mice (P21-27)**

mIPSCs were recorded in the presence of tetrodotoxin (1  $\mu$ M).

- A. Traces of mIPSCs, recorded in layer IV pyramidal cells of wt (*upper trace*) and *tg* (*lower trace*) mice. Holding potential -60 mV.
- B. Cumulative distributions for the mIPSP peak amplitude (*right*) and for the mIPSC inter-event intervals (*left*) in layer IV pyramidal cells of wt and *tg* mice.
- C. The median values of mIPSC amplitudes (*left*) and inter-event intervals (IEIs; *right*) of wt and *tg* mice. The mIPSC amplitudes and IEIs showed no significant difference between wt and *tg* mice.

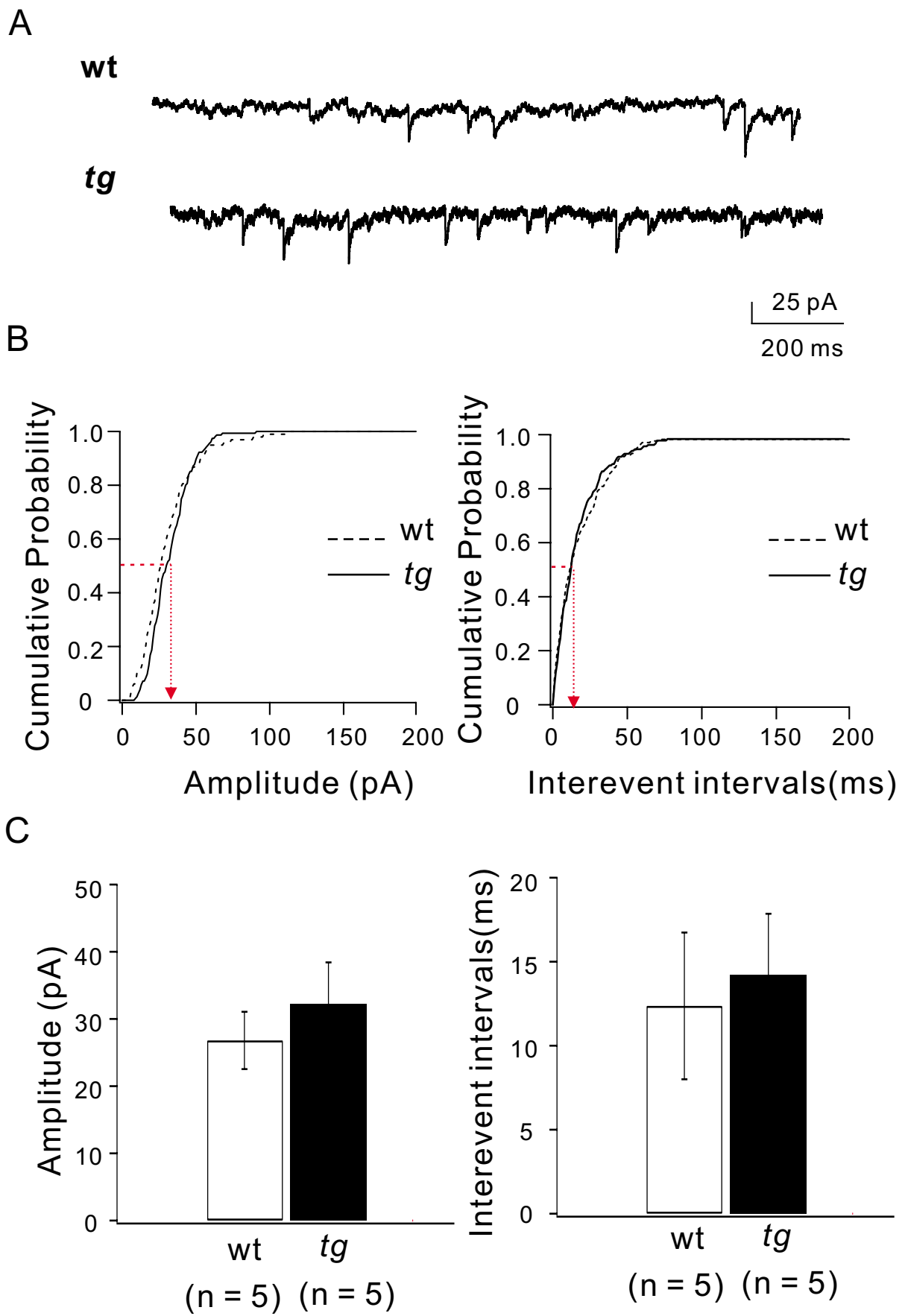


Fig.3.

**Fig.4. Distribution of inhibitory neurons and their axon terminals in the somatosensory cortex**

Distribution of inhibitory neurons and their axons in the layer IV of the somatosensory cortex was studied by an immunohistochemical method using anti-GAD antibody.

A. GAD-immunoreactive neurons in wt and *tg* mice (P21-23). There was no obvious difference in distribution of GAD-immunoreactive neurons in the barrel cortex between wt and *tg* mice. Arrows point to GAD-immunoreactive neurons. Scale bars 200  $\mu\text{m}$ .

B. Punctately stained GAD-immunoreactive axon terminals were observed around somata of large cells (indicated by the arrows). Scale bars 50  $\mu\text{m}$ .

C. Average density of GAD-immunoreactive cells showed no significant difference between wt and *tg* mice.

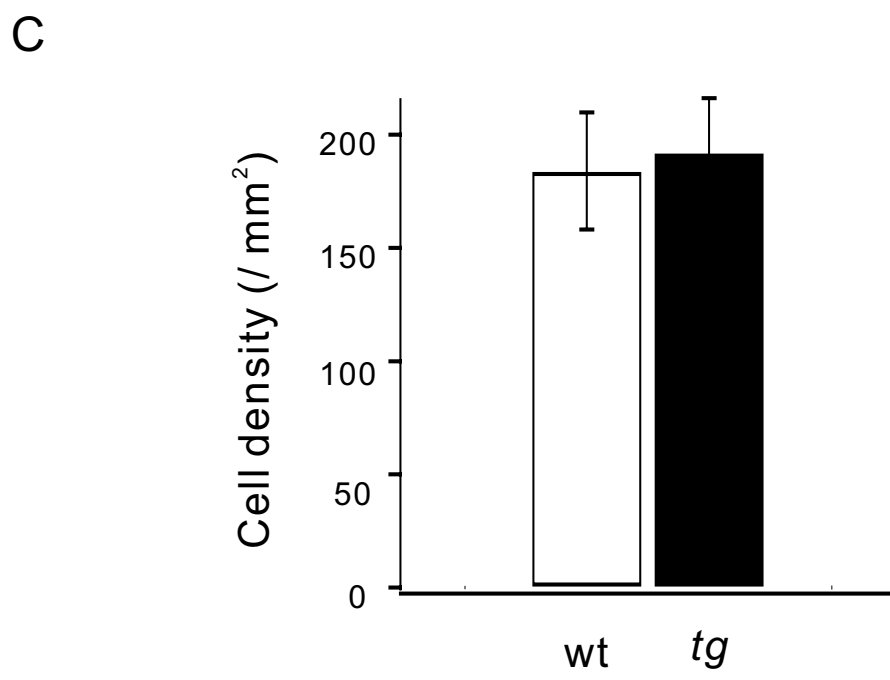
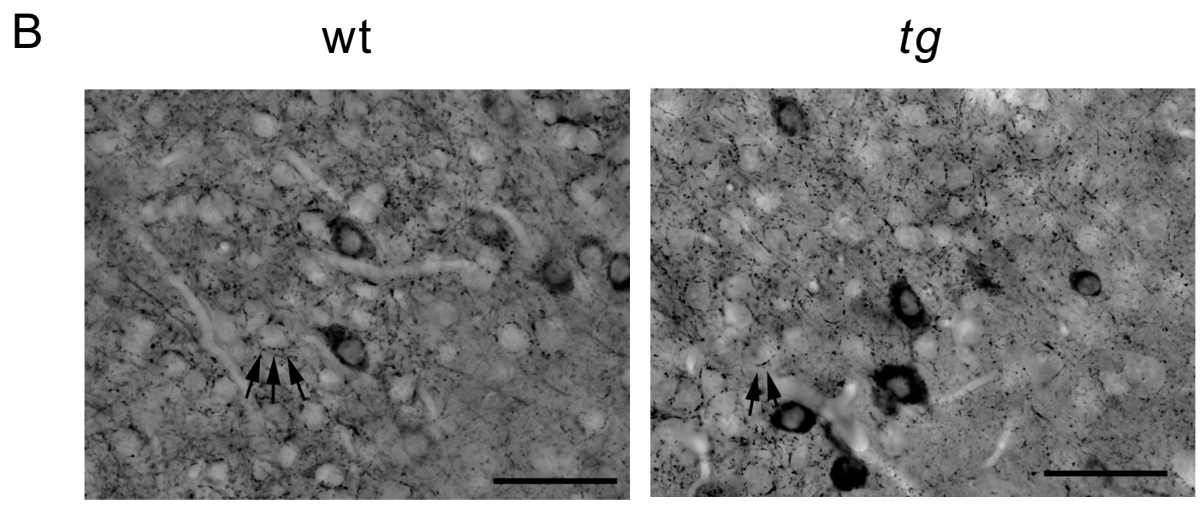
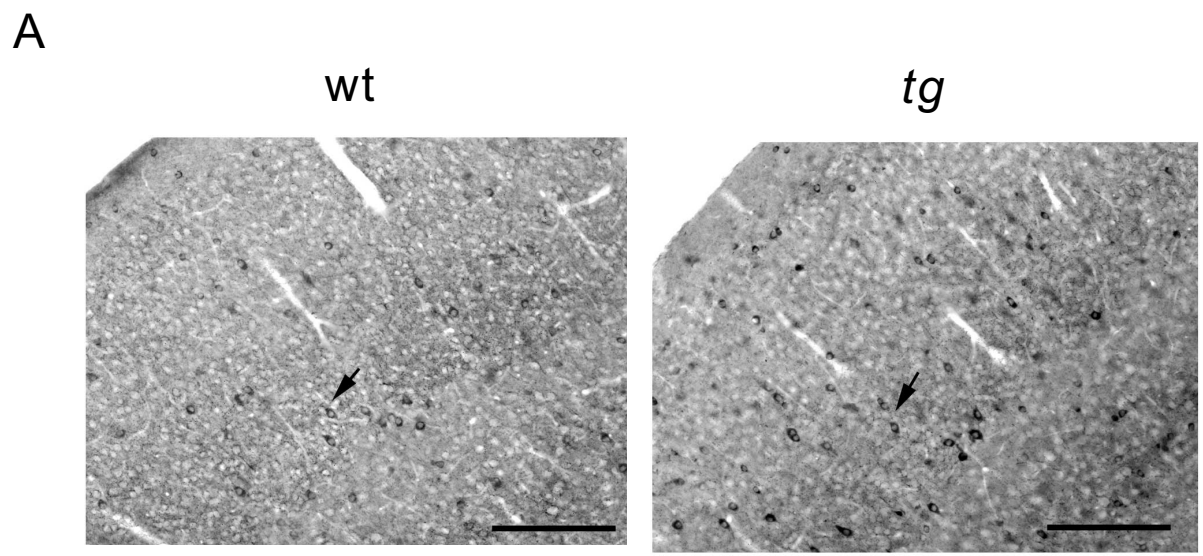


Fig.4.

**Fig.5. IPSCs recorded in layer V pyramidal cells of wt and *tg* mice (P21-30).**

IPSCs and EPSCs evoked by local stimulation were recorded in layer V pyramidal cells of wt and *tg* mice.

A. The IPSC peak amplitude was increased almost linearly with increments of the

stimulation intensity in layer V pyramidal cells of wt and *tg* mice. The insets show

IPSC traces by 1.0 mA stimulation. Each trace is an average of five recordings.

B. The EPSC amplitude in *tg* mice was mildly reduced. The insets show IPSC traces by

10 mA stimulation. Each trace is an average of five recordings.

C, D. Averaged IPSC peak amplitude with stimulation intensity of 1.0 mA (C) and

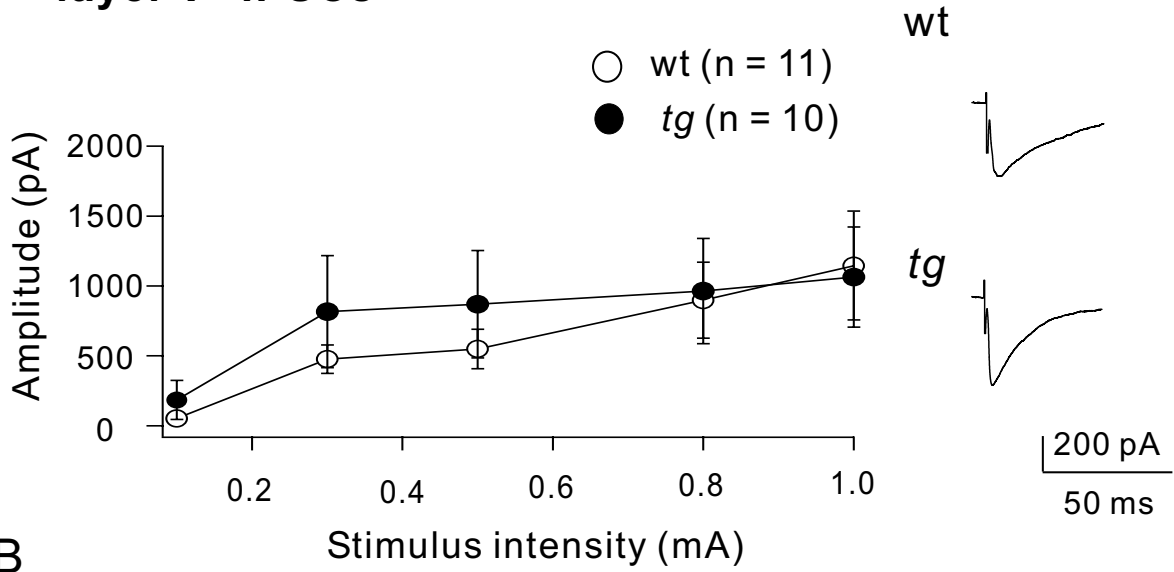
averaged EPSC peak amplitude with stimulation intensity of 10 mA (D) in layer V.

The averaged IPSC peak amplitude of *tg* was almost the same as that of wt, but the

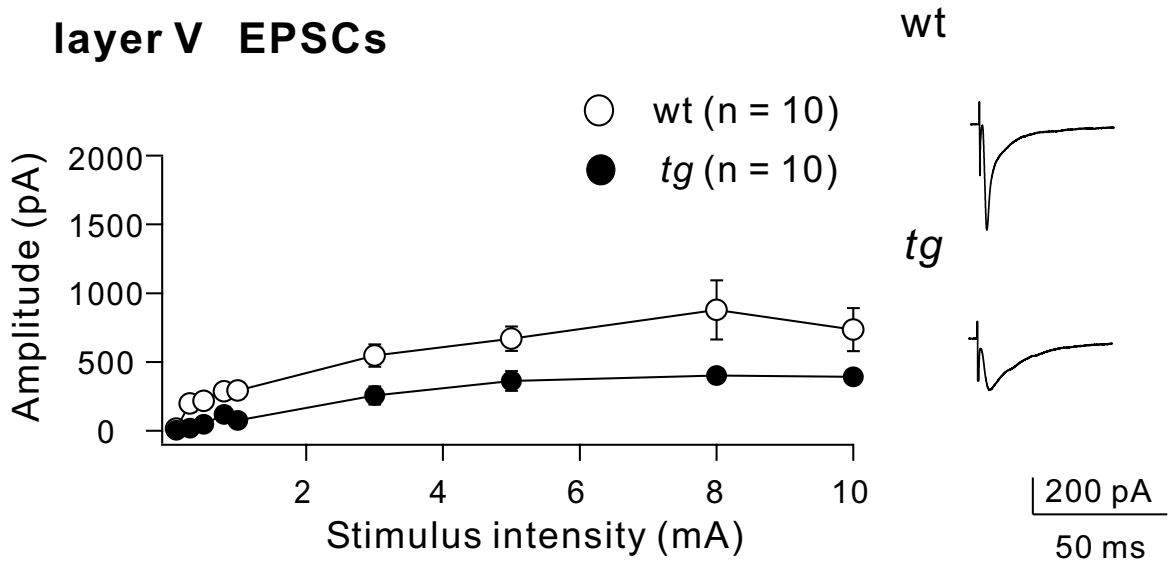
averaged EPSC peak amplitude reduced was mildly reduced in *tg* mice. The data

represent the means  $\pm$  SEMs.  $*p < 0.05$ .

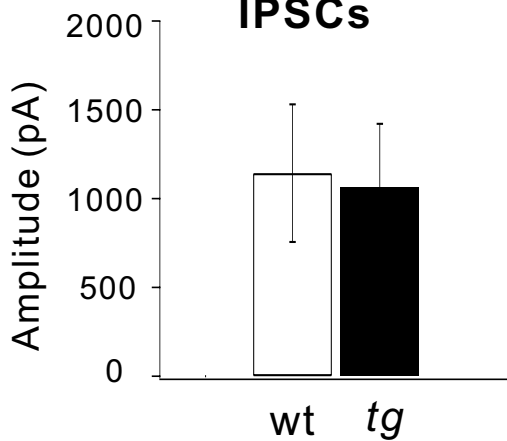
### A layer V IPSCs



### B layer V EPSCs



### C IPSCs



### D EPSCs

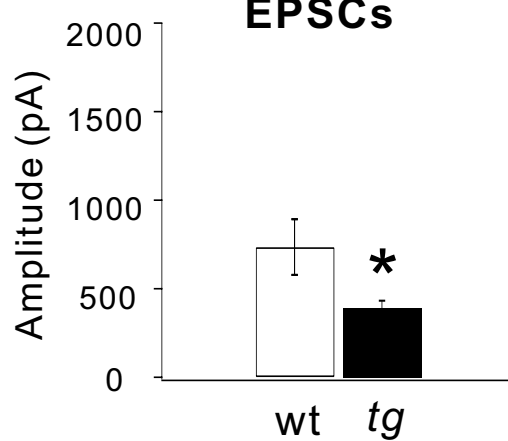


Fig.5.

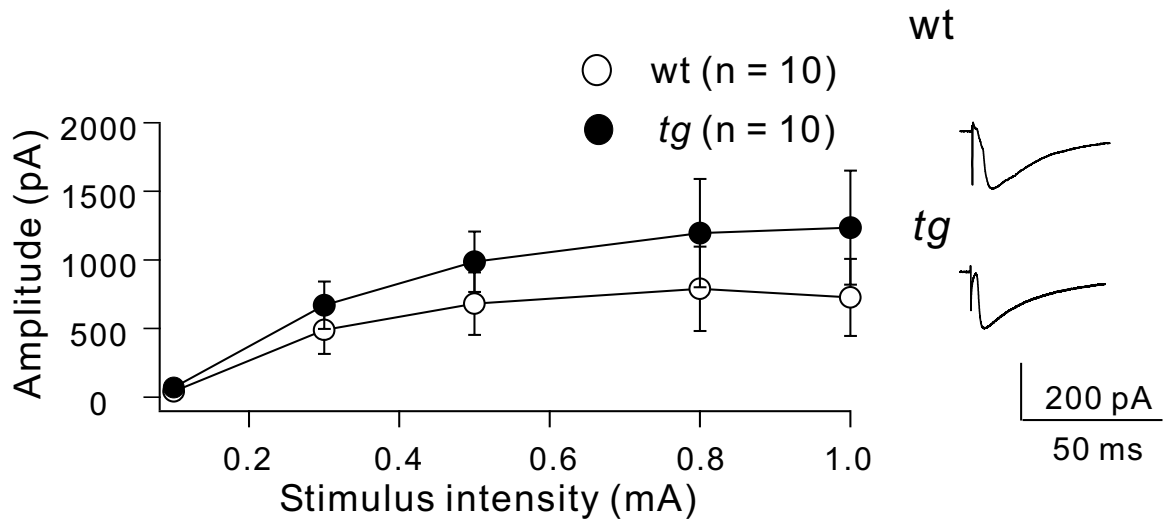
**Fig.6. IPSCs in layer IV and V pyramidal cells of younger wt and *tg* mice (P14-16)**

A, B. The IPSC peak amplitudes of layer IV (A) and V (B) were plotted against the intensity of stimulation for wt and *tg* mice at P14-16. In both layers, the IPSC peak amplitudes increased almost with increments of stimulation intensity in wt and *tg* mice. The insets show IPSC traces by 1.0 mA stimulation. Each trace is an average of five recordings.

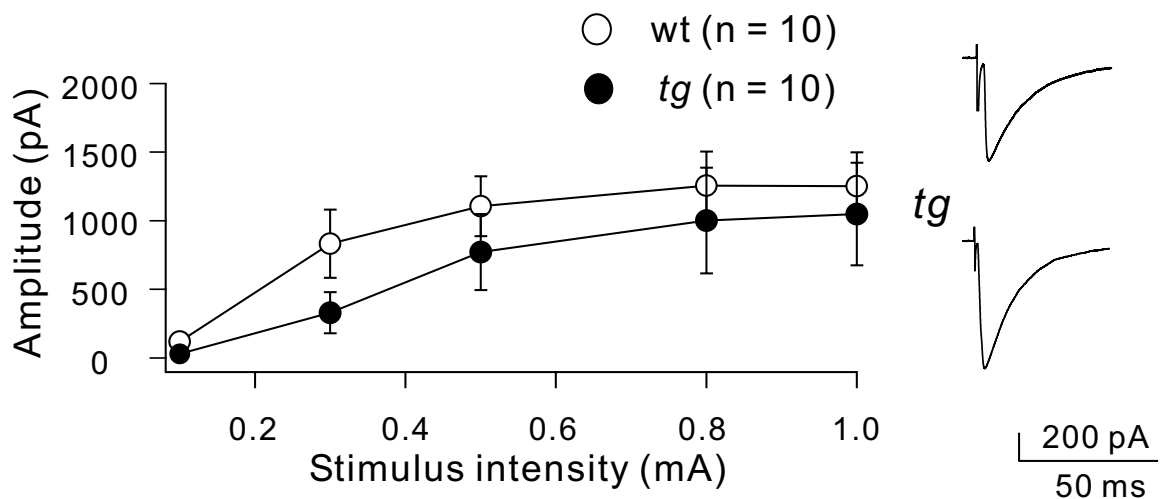
C, D. Averaged IPSC peak amplitudes (1.0 mA stimulation) of layer IV (C) and V (D).

The data represent the means  $\pm$  SEMs.

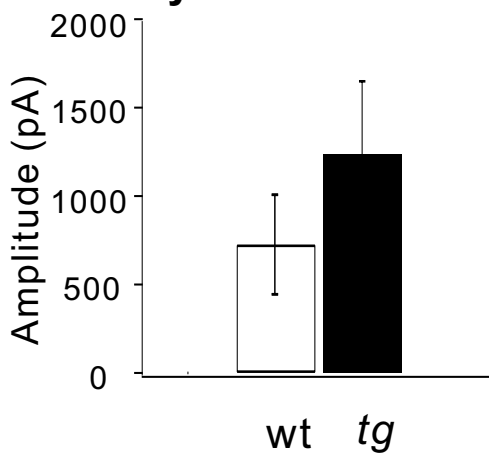
### A layer IV IPSCs (P14-16)



### B layer V IPSCs (P14-16)



### C layer IV IPSCs



### D layer V IPSCs

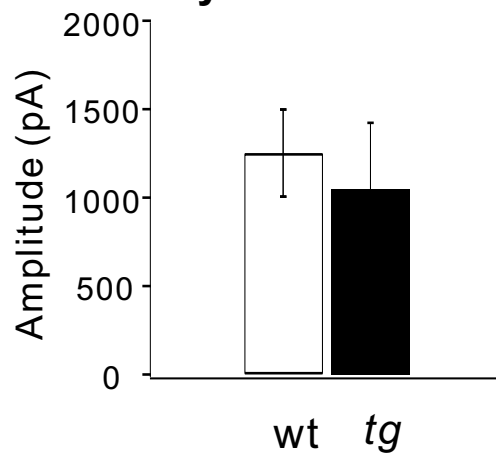


Fig.6.

**Fig.7. EPSCs in layer IV and V pyramidal cells of younger wt and *tg* mice (P14-16)**

A, B. The EPSC peak amplitudes of layer IV (A) and V (B) were plotted against the intensity of stimulation for wt and *tg* mice at P14-16. In both layers, the EPSC peak amplitudes increased almost linearly with increments of stimulation intensity in wt and *tg* mice. The insets show EPSC traces by 1.0 mA stimulation. Each trace is an average of five recordings.

C, D. Averaged EPSC peak amplitudes by stimulation of 1.0 mA of layer IV (C) and V (D). There was not statistically significant difference between wt and *tg* mice. The data represent the means  $\pm$  SEMs.

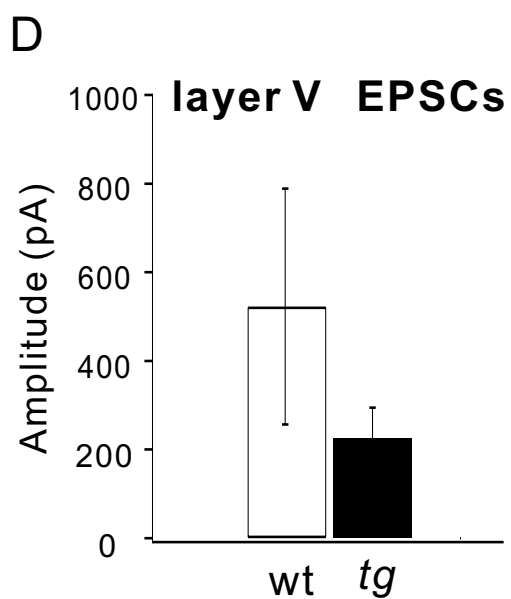
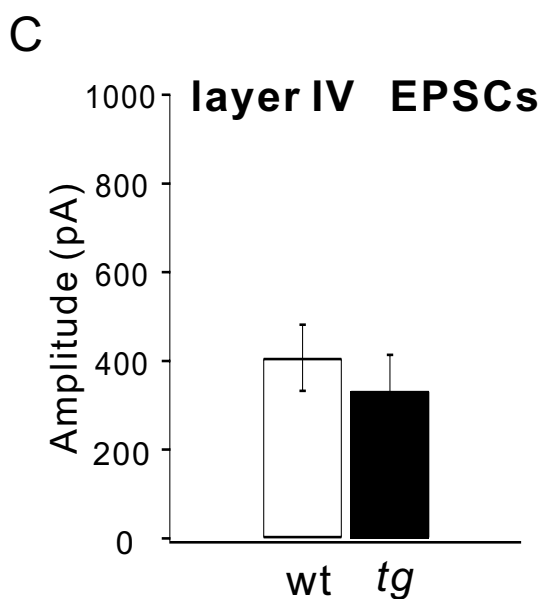
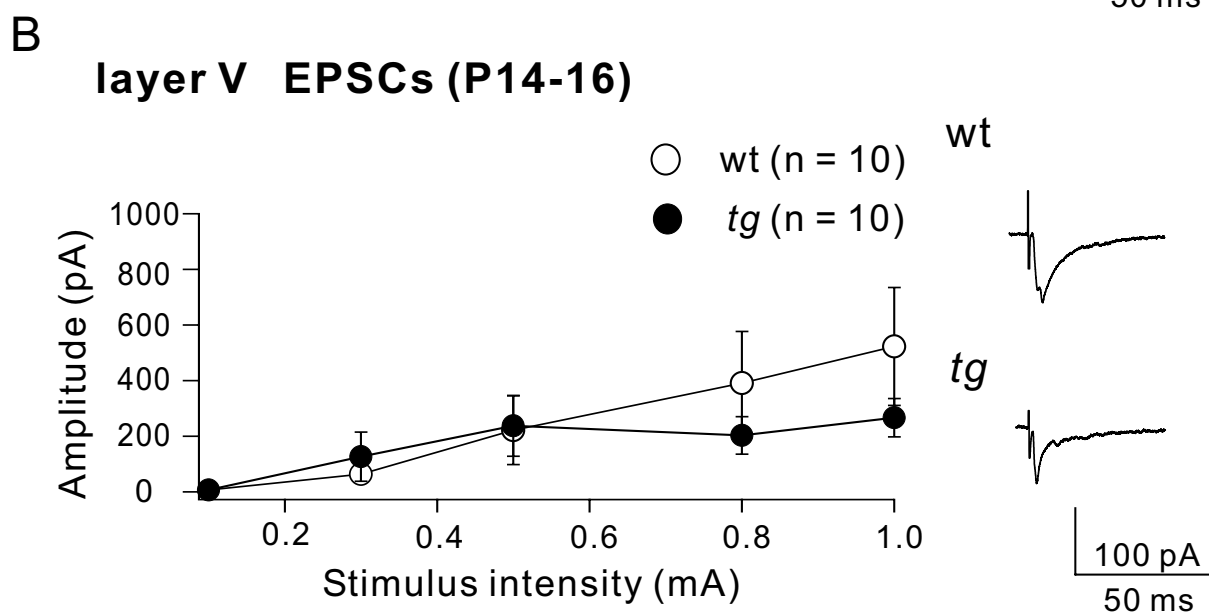
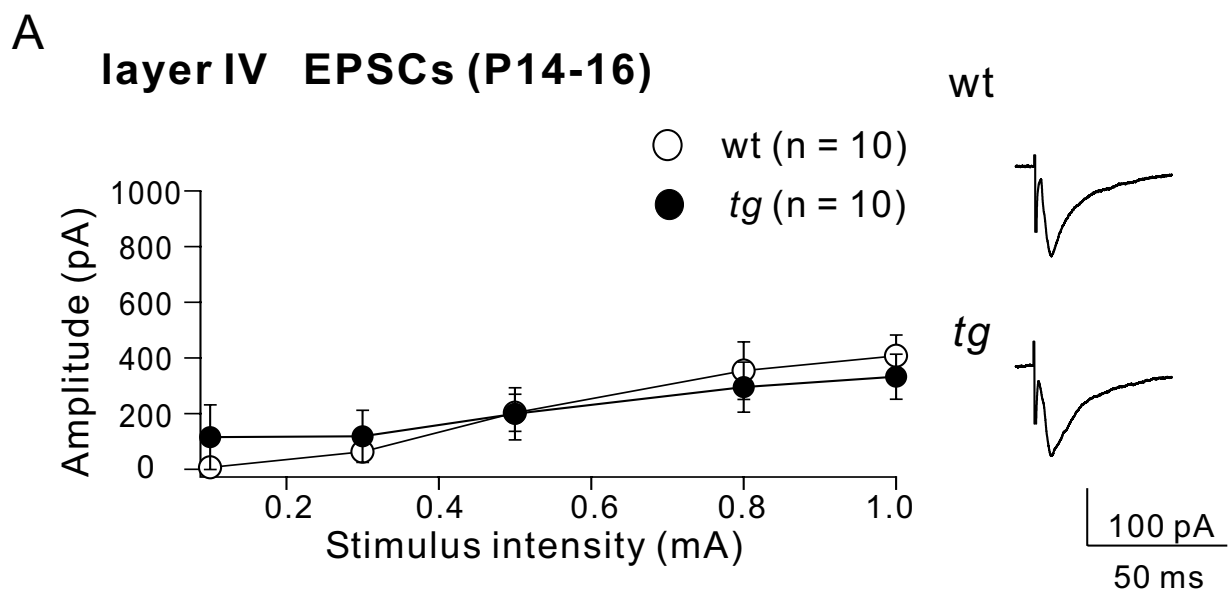


Fig.7.

**Fig.8. Developmental change in  $\omega$ -Aga-IVA sensitivity of IPSCs in layer IV**

**pyramidal cells**

A. Time course of the peak IPSC amplitude in response to application of  $\omega$ -Aga-IVA

(200 nM, *gray bar*) and  $\omega$ -CgTx (3  $\mu$ M, *white bar*).  $\omega$ -Aga-IVA (200 nM) reduced the IPSC amplitude by 19% at P14-15. The insets show IPSC traces at the time points indicated by the numbers. Each trace is an average of five recordings.

B.  $\omega$ -Aga-IVA (*gray bar*) reduced the IPSCs amplitude by 47%, and  $\omega$ -CgTx (*white*

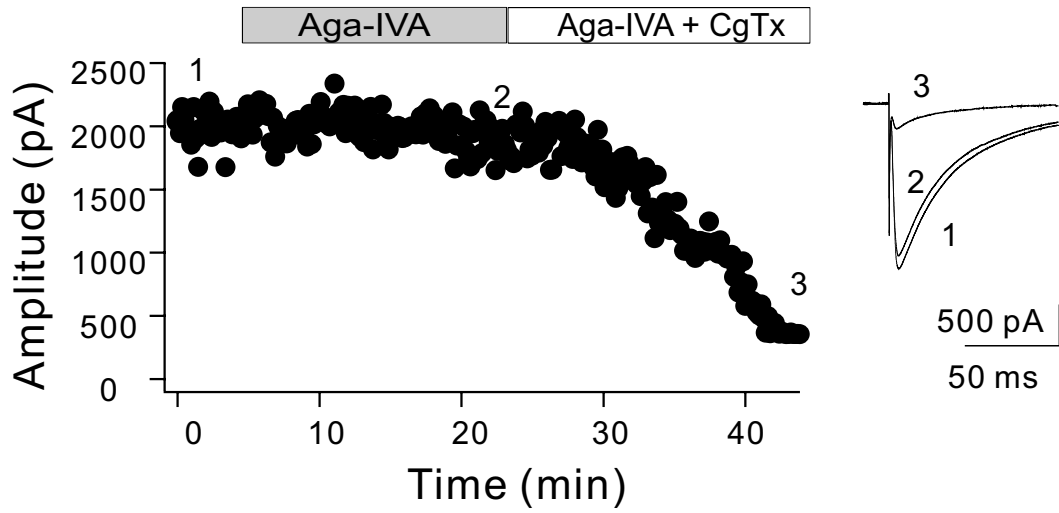
*bar*) almost completely blocked IPSCs at P21-22. The insets show IPSC traces at the time points indicated by the numbers. Each trace is an average of five recordings.

C. The IPSC fraction blocked by  $\omega$ -Aga-IVA at different postnatal ages. The data

represent the means  $\pm$  SEMs.  $**p < 0.01$

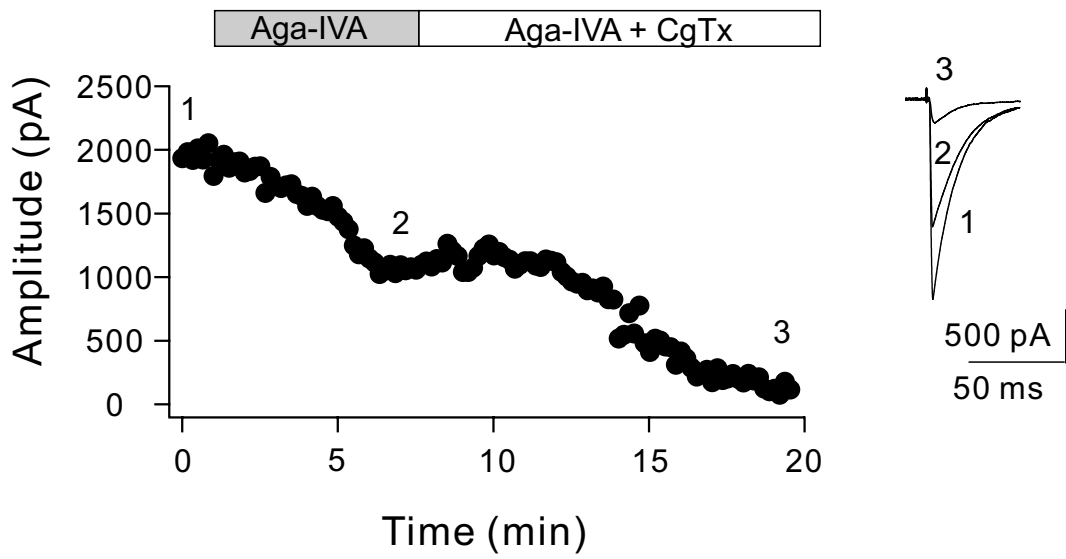
A

**P14-15**



B

**P21-22**



C

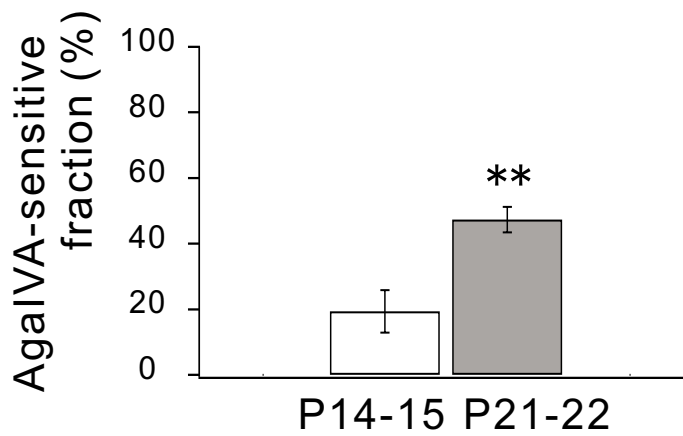


Fig.8.

**Fig.9. Multi-channel recordings and pharmacological characterization of evoked synaptic local field potentials (sLFP) in thalamocortical slices.**

sLFP evoked by local stimulation in layer IV were recorded by an MED64 multi-channel recording system.

A. Placement of an MED64 electrode array with the inter-electrode spacing of 100  $\mu\text{m}$  (scale bar 500  $\mu\text{m}$ ). The top row of electrodes was placed in free space, so that we could judge whether responses were artifact or real.

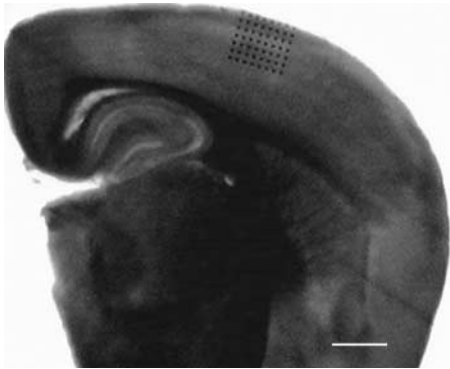
B. sLFP induced by stimulus (0.2 mA for 0.1 msec) were recorded (average over 10 sweeps). The asterisk indicates the location of the stimulating microelectrode, which was in the center of a barrel.

C. Spatial activity map of the sLFP signals of the recording shown in B, at 5 ms after stimulation. The location of stimulation is indicated by a black circle.

D. Identification of the postsynaptic response in the sLFP (*black trace*). The postsynaptic component was completely abolished after blocking the synaptic transmission with 5 mM  $\text{Co}^{2+}$  (*green trace*).

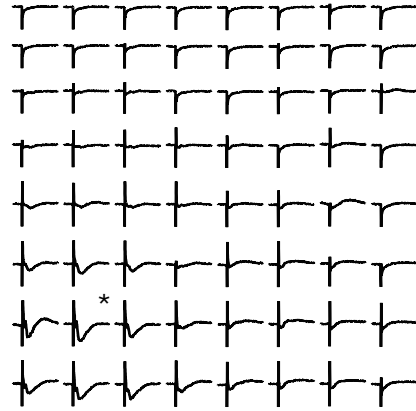
- E. Effect of picrotoxin. The negative component became larger by 50  $\mu$ M picrotoxin (*red trace*) than the control trace in ACSF (*black trace*). The negative component disappeared after additional application of 10  $\mu$ M CNQX and 100  $\mu$ M APV (*blue trace*).
- F. The negative component recorded in ACSF (*black trace*) was almost completely blocked by CNQX and APV (*blue trace*).

A



500  $\mu\text{m}$

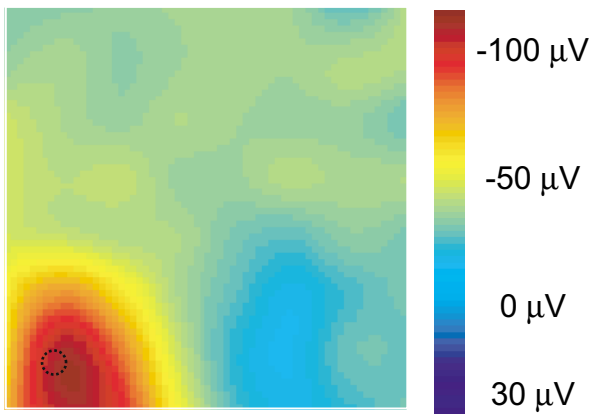
B



50  $\mu\text{V}$   
5 ms

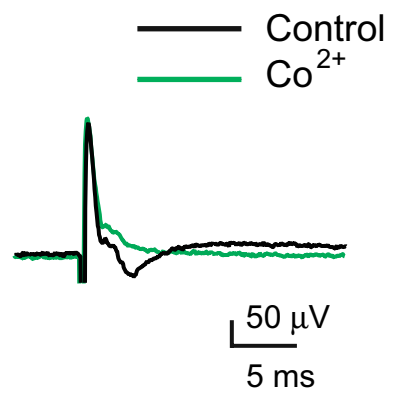
C

at 5ms



100  $\mu\text{m}$

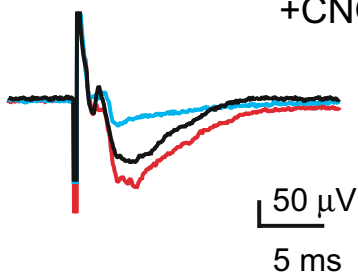
D



50  $\mu\text{V}$   
5 ms

E

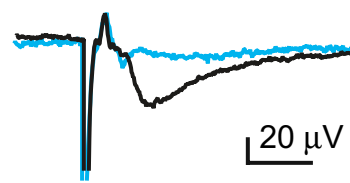
Control  
Picrotoxin  
Picrotoxin  
+CNQX+APV



50  $\mu\text{V}$   
5 ms

F

Control  
CNQX+APV



20  $\mu\text{V}$   
5 ms

Fig.9.

**Fig.10. Spreading of neuronal excitation in layer IV of wt and *tg* at P21-30**

A. Time course of activity maps is shown using a pseudocolor coding, with red showing the highest activity. The recorded time is indicated above each panel.

B. The normalized sLFP amplitude at recording sites at 100  $\mu\text{m}$  and further away from stimulus location was clearly increased in *tg* mice. This difference did not change even if the stimulation intensity was increased (up to 50  $\mu\text{A}$  above the minimum stimulation).

C. The normalized sLFP amplitudes at various distances from the stimulus location were compared between wt and *tg* mice. The spreading of excitation in the horizontal directions in layer IV at 100  $\mu\text{m}$  was significantly stronger away in *tg* than in wt mice. The data represent the means  $\pm$  SEMs.  $**p < 0.01$ .

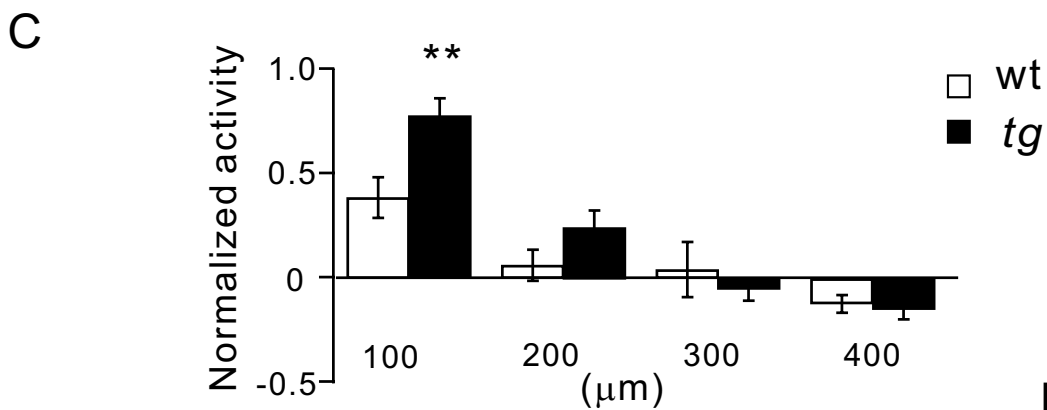
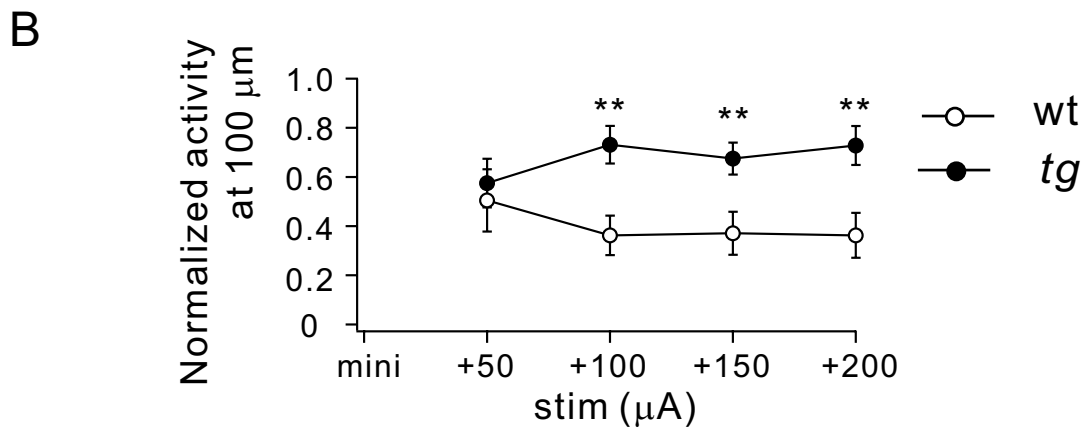
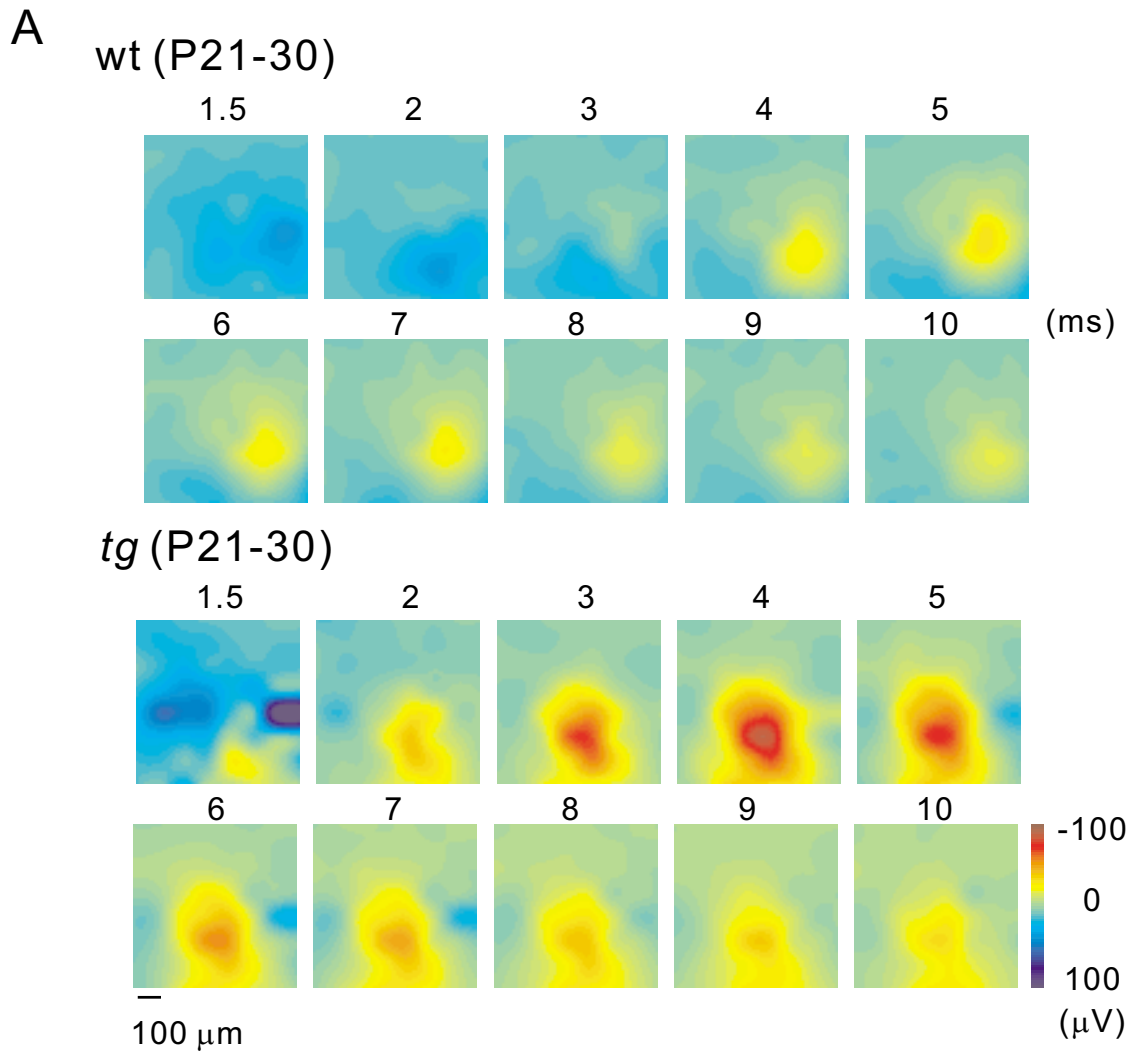


Fig.10.

**Fig.11. Spreading of neuronal excitation in layer IV of wt and *tg* at P14-16**

A. Time course of activity maps after stimulation. The recorded time is indicated above each panel for wt and *tg* mice.

B. The normalized sLFP amplitudes at recording sites at 100  $\mu\text{m}$  and further away from stimulus location were not statistically different in wt and *tg* mice with various stimulation intensities.

C. No significant differences in the width of the excitation were observed between wt and *tg* mice. The data represent the means  $\pm$  SEMs.

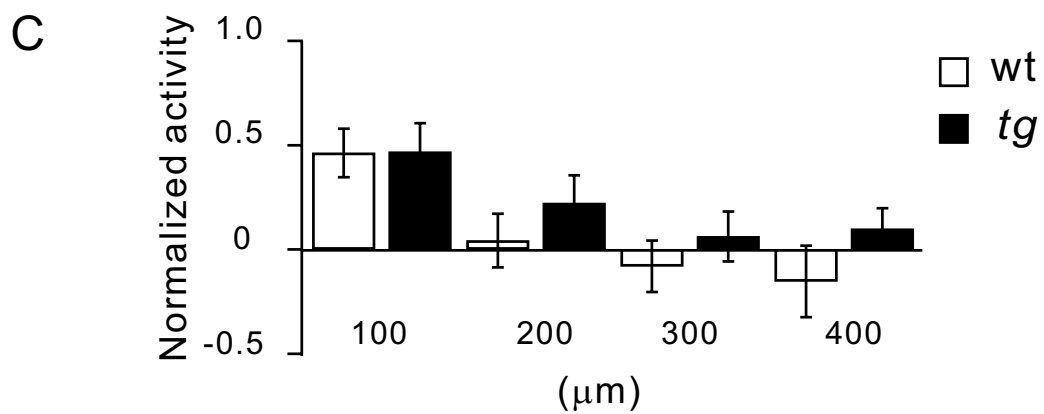
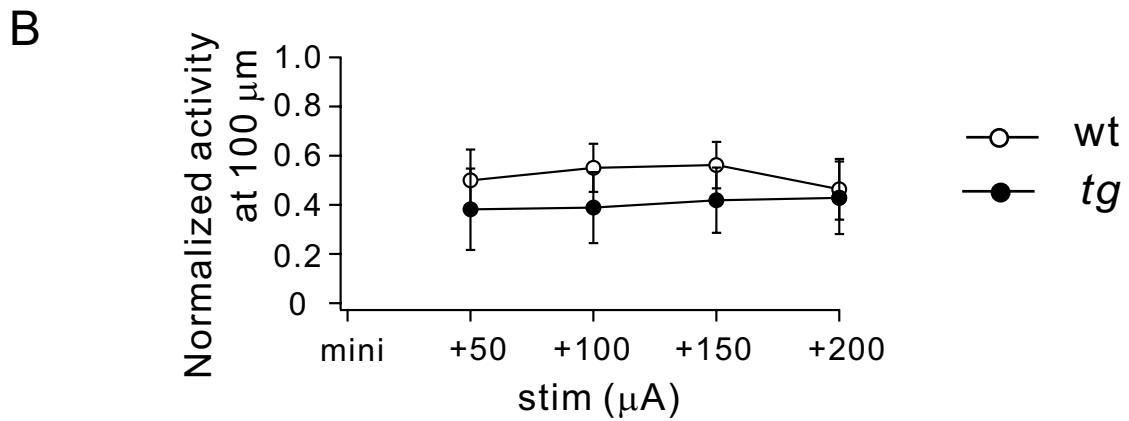
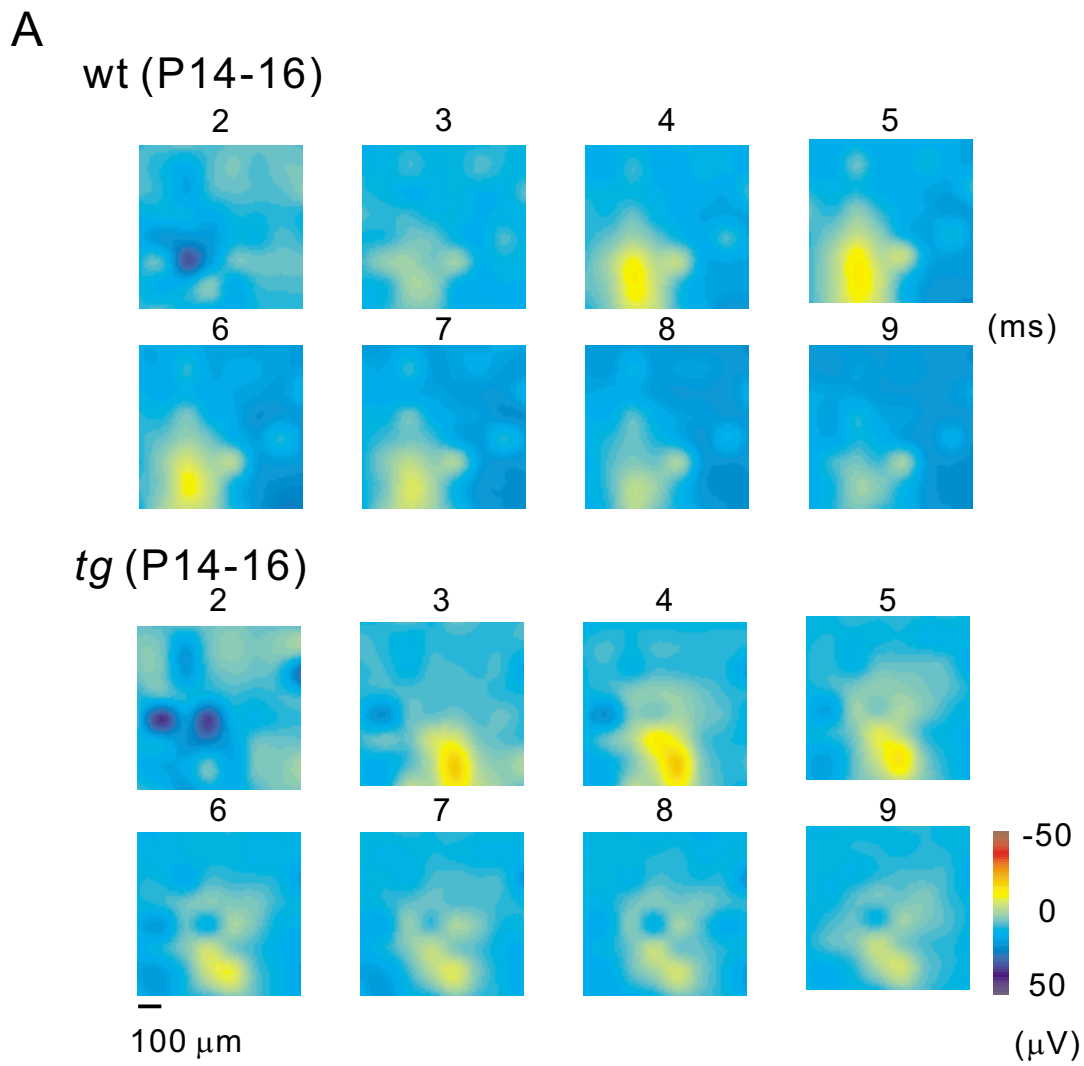


Fig.11.